Portals into Higgs vacuum stability

Gudrun Hiller,[1] Tim Höhne,[1] Daniel F. Litim,[2] and Tom Steudtner[1,2]
[1]*Department of Physics, TU Dortmund University, Otto-Hahn-Strasse 4, D-44221 Dortmund, Germany*
[2]*Department of Physics and Astronomy, University of Sussex, Brighton BN1 9QH, United Kingdom*

(Received 22 July 2022; accepted 11 November 2022; published 5 December 2022)

We address the notorious metastability of the Standard Model (SM) and promote it to a model building task: What are the new ingredients required to stabilize the SM up to the Planck scale without encountering sub-Planckian Landau poles? Using the SM extended by vectorlike fermions, we chart out the corresponding landscape of Higgs stability. We find that the gauge portal mechanism, triggered by new SM charge carriers, opens up sizable room for stability in a minimally invasive manner. We also find models with Higgs criticality and Yukawa portals opening up at stronger coupling. Several models allow for vectorlike fermions in the TeV range, which can be searched for at the LHC. For nontrivial flavor structure, severe flavor-changing neutral current constraints arise that complement those from stability and push lower fermion masses up to $\mathcal{O}(10^3\ \mathrm{TeV})$.

DOI: 10.1103/PhysRevD.106.115004

I. INTRODUCTION

The discovery of the Higgs particle [1,2] a decade ago, together with theoretical precision calculations [3,4] evidenced the instability of the Standard Model (SM) vacuum. While a theory of nature with a decaying ground state would be unacceptable, vacuum metastability due to a lifetime sufficiently large compared to the age of the Universe has become a widely accepted narrative. Moreover, it is expected that new physics prior to the scale of metastability ($\mu_{\rm inst} \approx 10^{10}$ GeV), and possibly not too far above the TeV scale, may stabilize the ground state. This view has been confirmed in many scenarios for physics beyond the SM (BSM), for instance [5–81]. On the other hand, much less attention has been given to vacuum stability in its own right.

In this work, we propose a change of perspective by bringing the SM instability into the fore and promoting it into a primary model building task. There are several reasons for doing so now:

(i) The continuous success of the SM in the LHC era with only a few anomalies, and the absence of clear new physics signatures at colliders or elsewhere, calls for new theory ideas and directions in model building.
(ii) The onset of the SM instability is a high energy effect and out of reach for future colliders. However, the existence of the instability is not directly pointing at a mass scale for new physics. Its remedy, therefore, may arise from new phenomena at any scale below the Planck scale and possibly from scales as low as a few TeV. The latter opens a door for indirect tests of stability at present and future colliders.
(iii) Understanding the RG running of couplings and masses between TeV and the Planck scale with high precision is key for testing vacuum stability beyond the SM. Powerful and versatile computer-algebraic tools such as ARGES [82] have become available, which offer easy access to advanced perturbative beta functions for any 4D QFT and SM extension.

In this spirit, we investigate ingredients and mechanisms required to reinstate stability. We will be satisfied if this happens at and possibly the whole way up to the Planck scale where quantum gravity is expected to kick in. In addition, we demand that the renormalization group (RG) running of couplings up to the Planck scale remains finite and well defined, without encountering any singularities or Landau poles along the way. We focus on SM extensions by vectorlike fermions (VLFs) and the study of gauge portals—which arise because new SM gauge charge carriers are available and Yukawa portals—which arise as soon as the new fermions admit new Yukawa couplings with SM matter. Our main interests are the constraints dictated by stability on BSM matter fields, their masses, multiplicities, or interactions. We are particularly interested in settings where stability arises through effects at the TeV scale, which can be probed at colliders.

The paper is organized as follows: We recall the state of affairs in the SM and basic strategies toward stability (Sec. II). We then explain why and how the gauge portal mechanism provides stability in a minimally invasive

manner (Sec. III). We further include Yukawa interactions and contrast the availability of gauge versus Yukawa stability portals and discuss phenomenology (Sec. IV). We conclude in Sec. V.

II. VACUUM STABILITY

A. Standard model

We begin by taking stock of Higgs stability in the SM. To that end, we plot the three-loop running of SM couplings up to the Planck scale and beyond (Fig. 1). We also introduce the $U(1)_Y \times SU(2)_L \times SU(3)_c$ gauge couplings $g_\ell (\ell = 1, 2, 3)$, Yukawa interactions Y, and the Higgs quartic λ, all normalized in units of loop factors, and write them as

$$\alpha_\ell = \frac{g_\ell^2}{(4\pi)^2}, \qquad \alpha_Y = \frac{Y^2}{(4\pi)^2}, \qquad \alpha_\lambda = \frac{\lambda}{(4\pi)^2}. \quad (1)$$

Because of their smallness, SM Yukawas other than those of the top (y_t) and bottom (y_b) are immaterial for the RG evolution and can be safely neglected, corresponding to the approximation

$$Y^u_{ij} = y_t \delta_{i3}\delta_{j3}, \qquad Y^d_{ij} = y_b \delta_{i3}\delta_{j3}, \qquad Y^\ell_{ij} = 0 \quad (2)$$

for the up and down quark as well as the charged lepton Yukawa matrices, respectively. SM initial conditions (central values) at the reference scale $\mu_0 = 1$ TeV are determined as

$$\begin{aligned}
\alpha_1(\mu_0) &= 8.30 \times 10^{-4}, \\
\alpha_2(\mu_0) &= 2.58 \times 10^{-3}, \\
\alpha_3(\mu_0) &= 7.08 \times 10^{-3}, \\
\alpha_\lambda(\mu_0) &= 6.09 \times 10^{-4}, \\
\alpha_t(\mu_0) &= 4.61 \times 10^{-3}, \\
\alpha_b(\mu_0) &= 1.22 \times 10^{-6}. \quad (3)
\end{aligned}$$

The uncertainties [4] in the initial values (3) due to the strong gauge coupling, Higgs, and W mass are quantitatively irrelevant. The dominant source of uncertainty originates from the determination of the top mass [83]

$$m_t = 172.76 \pm 0.30 \text{ GeV}. \quad (4)$$

We then have integrated the SM renormalization group equations (RGEs) from the TeV scale up to the hypercharge Landau pole (Fig. 1). Because of its smallness, the bottom Yukawa $\alpha_b(\mu)$ is not displayed but is included in the numerics. We observe that most SM couplings run slowly. We have also indicated the 1σ uncertainty band (4) for all couplings. In practice the bandwidth is visible only for the Higgs quartic (violet band), which takes higher (lower) values for a smaller (larger) top mass. The Higgs quartic invariably changes sign ($\mu \approx 10^{10}$ GeV) and the vacuum becomes unstable, signaled by the downward spike prior to the Planck scale (gray band). Stability at the Planck scale would require that the top mass deviates by more than 3σ from its presently determined central value. This suggests that a negative value for the Higgs quartic at the Planck scale and the possibility of an unstable "great desert" should be taken for real.

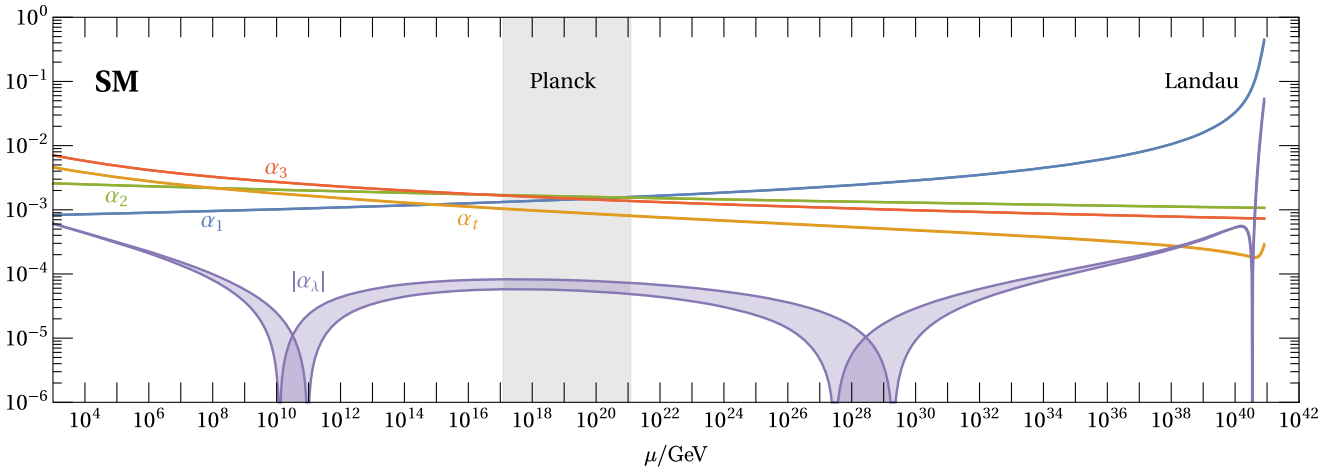

FIG. 1. Shown is the running of the Higgs, top Yukawa, and gauge couplings in the Standard Model between the TeV and the Planck scale (gray band) and further up to the Landau pole of the hypercharge coupling where the running breaks down. The SM vacuum becomes unstable around $\mu \approx 10^{10}$ GeV and remains so up to the Planck scale, with the largest source of uncertainty arising from the top pole mass (4), indicated by 1σ-band widths for all couplings (see main text).

Taking the liberty of ignoring quantum gravity effects, we extend the SM flow into the trans-Planckian regime. Perhaps unexpectedly, we find that the Higgs becomes stable again ($\mu_{\rm stab} \approx 10^{10} M_{\rm Pl}$), with the second sign change largely triggered by the mild but continued growth of the hypercharge coupling. The vacuum becomes fully unstable at higher scales ($\mu \approx 10^{23} M_{\rm Pl}$), shortly before the hypercharge Landau pole is reached, which finally brings down the SM as we know it.

We conclude that new effects are required to stabilize the vacuum, either at the Planck scale, such as from higher-dimensional operators [84] or fully fledged quantum gravity, or from below the Planck scale, such as from new particles or interactions.

B. Portals

Next, we are interested how vacuum stability can be improved using low-scale BSM mechanisms, some of which can be tested at colliders.

The perhaps simplest such mechanism consists in the addition of BSM fermions ψ in a nontrivial representation under the $U(1)_Y \times SU(2)_L \times SU(3)_c$ SM gauge group. The main effect of these "gauge portals"

$$\mathcal{L} \supset \bar{\psi} i \not{D} \psi \tag{5}$$

arises through modifications of the RG running of SM interactions. The exploration of gauge portals, a main novelty of this work, is given in Sec. III.

Alternatively, "Yukawa portals" arise when the Higgs couples directly to a BSM fermion ψ and a SM fermion $f_{\rm SM}$,

$$\mathcal{L} \supset -\kappa \bar{\psi} H f_{\rm SM}. \tag{6}$$

Unlike the gauge portals that solely involve new SM charge carriers, Yukawa portals are additionally controlled by new Yukawa interactions κ. In general, Yukawa portals are flavorful with three SM generations $j = 1, 2, 3$ and a BSM flavor index $i = 1, \ldots, N_F$. These interactions allow the ψ to decay to SM particles and avoid potential issues with otherwise too long-lived VLFs. To leading loop order, Yukawa couplings contribute to the running of the Higgs quartic as

$$\beta_\lambda = \beta_\lambda^{\rm SM} + I_{\kappa\lambda} \alpha_\kappa \alpha_\lambda - I_{\kappa\kappa} \alpha_\kappa^2 + \mathcal{O}(\text{two} - \text{loop}), \tag{7}$$

where both $I_{\kappa\lambda}, I_{\kappa\kappa} > 0$ [74,85]. Sufficiently small α_κ does not spoil stability as it induces a positive one-loop contribution to the beta function of the quartic. However, once $\alpha_\kappa \gtrsim \alpha_\lambda$, which is bound to happen if the Higgs potential becomes very flat, the second term takes over and starts to destabilize the vacuum. It has also been observed that the Yukawa portal can stabilize the Higgs at larger coupling through a walking regime.[1] In addition, the Yukawa portal to the Higgs always implies a gauge portal (5), and their interplay is analyzed in Sec. IV. We also note that several BSM Yukawas with H can arise if several suitable representations of BSM fermions exist, say ψ and χ, allowing for additional Yukawa portals such as $\bar{\psi} H \chi$.

Finally, in the presence of BSM scalars, "Higgs portals" arise as soon as the Higgs H couples to the BSM scalar S through a portal coupling δ,

$$\mathcal{L} \supset -\delta S^\dagger S H^\dagger H. \tag{8}$$

This new portal interaction improves vacuum stability as it provides a positive one-loop contribution to the running of the Higgs quartic $\beta_\lambda \approx \beta_\lambda^{\rm SM} + I_\delta \alpha_\delta^2$ and $I_\delta > 0$ [74,85]. Also, Higgs portals come along with gauge portals (5) provided the BSM scalar is charged under the SM; see [74] for models with gauge, Higgs, and Yukawa portals simultaneously.

Previous works have studied vacuum stability from the viewpoint of concrete BSM models. These include SM extensions by single uncharged real [15,35,36,60], complex [5–7,12,16,17], or charged scalars such as leptoquarks [52,80] or other [33,76]. Many works feature both scalar and fermionic BSM fields, such as type I [34,37,73], type II [13,53,54,58], type III [37,62], and inverse seesaw models [38,77], as well as theories with matrix scalar fields [39,71,74,81] or models with uncharged scalars coupling to charged BSM fermions [18,30–32,63,75]. More complex extensions include two-Higgs-doublet models, e.g., [28,40–44,51,64,72], $U(1)'$ extensions [14,19,20,29,45–48,50,59,65,81], or extended dark gauge sectors [23], grand unified theories (GUTs) [21,49,55,66,67,70,78], and many others [22,24–26,56,57,61,69,79]. Extensions that rely solely on BSM fermions are less common; notable exceptions include [8–11,27,68].

In this work, we systematically explore SM extensions with N_F VLFs of mass M_F and charged under the $U(1)_Y \times SU(2)_L \times SU(3)_c$ SM gauge group. By design, all models are free of gauge anomalies and allow for direct Dirac mass terms. Our setup gives access to gauge portals (5), which we discuss in Sec. III, and to gauge-Yukawa portals (6), which we discuss Sec. IV. To test vacuum stability quantitatively, we match SM extensions onto the SM at the mass scale of the BSM fermions, which we take to be in the TeV range or above,

$$\mu_0 = M_F \gtrsim 1 \text{ TeV}. \tag{9}$$

[1]Walking regimes refer to a parametrically slowed-down running of gauge couplings due to a near zero of their beta functions, e.g., [86,87]. More recently, walking regimes have also been observed in Yukawa and scalar sectors [71,74,81].

SM couplings are matched to their BSM counterparts via

$$\alpha^{\rm BSM}_{1,2,3,t,b,\lambda}(\mu_0) = \alpha^{\rm SM}_{1,2,3,t,b,\lambda}(\mu_0). \tag{10}$$

We briefly comment on threshold corrections, which are neglected in this work. In principle, threshold corrections arise at loop level and replace the dependence on the unphysical matching scale μ_0 by the physical mass M_F (see, e.g., [88] for a pedagogical introduction). One-loop thresholds to the gauge couplings are well known to be $\propto \ln\frac{\mu_0}{M_F}$ [89] and therefore vanish as we match at $\mu_0 = M_F$, see (9). Moreover, for BSM fermions that solely interact with the SM gauge sector, threshold corrections to the SM Yukawas and Higgs self-interaction only start at two loops. Consequently, our matching procedure (10) only neglects threshold corrections that are suppressed by two-loop orders and higher.

We employ the tool ARGES [82] to generate the two-loop β functions for all running couplings, which are then integrated numerically between the scale of new physics μ_0 and the Planck scale. The goal is to identify the set of BSM parameters such as the mass scale M_F and the field multiplicities where the RG flow remains well-defined without Landau poles and the vacuum becomes stable at the Planck scale. We refer to this set of parameters as the "BSM critical surface."

As a side aspect, we also watch out for settings where the Higgs coupling remains stable all the way up to the Planck scale, as opposed to settings where it may have changed its sign (say, twice) along the trajectory up to the Planck scale. The former stipulates that loop corrections, resummed by the RG evolution, may not overturn the tree-level condition at any scale. The latter seeks to minimize radiative corrections to the resummed potential by imposing stability at the highest scale.[2]

III. GAUGE PORTALS

In this section we introduce and explain the mechanism of gauge portals for vacuum stability. We then illustrate the different gauge portals quantitatively by looking into concrete extensions of the SM and their main features and characteristics.

A. Gauge portals at work

We begin by explaining why gauge portal mechanisms can stabilize the Higgs potential in a minimally invasive manner. The essence of the mechanism is the addition of N_F vectorlike fermions of mass M_F, charged under the SM gauge group as

$$(Y_F, d_2, d_3) \tag{11}$$

and without adding any new interactions. The latter can be achieved either by specific choices of representations that forbid Yukawa interactions with SM fields, or by noting that Yukawa couplings are natural and cannot be switched on through quantum fluctuations. The net primary effect of the new matter fields is a modification of the running gauge couplings. Modifications to the running of the Higgs quartic, which is the ultimate goal of the mechanism, are much milder in that they only arise indirectly, namely, through a modified running of the top Yukawa and the gauge couplings and without changing the beta function itself.

To understand the gauge portal mechanism more quantitatively, we start with the running of the gauge couplings at one loop,

$$\beta_i \approx -B_i \alpha_i^2. \tag{12}$$

Integrating the flow between the matching scale μ_0 and some higher scale Λ, we find

$$\alpha_i(\Lambda) = \frac{\alpha_i(\mu_0)}{1 + \alpha_i(\mu_0) B_i \ln\left(\frac{\Lambda}{\mu_0}\right)}. \tag{13}$$

The one-loop gauge coefficients

$$\begin{aligned} B_1 &= -\frac{41}{3} - \delta B_1, \\ B_2 &= \frac{19}{3} - \delta B_2, \\ B_3 &= 14 - \delta B_3, \end{aligned} \tag{14}$$

contain the SM contributions, while the BSM contributions (11) are hidden in the coefficients $\delta B_i \geq 0$, which read

$$\begin{aligned} \delta B_1 &= \frac{8}{3} N_F d_2 d_3 Y_F^2, \\ \delta B_{2,3} &= \frac{8}{3} N_F d_{3,2} S_2(d_{2,3}). \end{aligned} \tag{15}$$

Here, $S_2(d_{2,3})$ denote the respective Dynkin indices of the $SU(2)_L$ and $SU(3)_c$ representations. If BSM fields are integrated out at the matching scale μ_0, the gauge couplings generically take larger values than the SM running at a high scale $\Lambda > \mu_0$. Using (13), we have

$$\frac{1}{\alpha_i(\Lambda)} - \frac{1}{\alpha_i^{\rm SM}(\Lambda)} = -\delta B_i \ln\left(\frac{\Lambda}{\mu_0}\right) < 0 \tag{16}$$

in comparison with the running in the SM.

[2]In our models, if a quartic changes sign twice prior to the Planck scale, it still remains larger than in the SM ($\alpha_\lambda \simeq -10^{-4}$), see Fig. 1. Hence, models are always less unstable than the SM or even outright stable due to positive quartics at the Planck scale [see Fig. 7 for examples]. Stability can further be confirmed by computing the full Higgs effective potential.

Next, we turn to the top Yukawa coupling. Owing to its magnitude in the SM, it plays a significant role for the stability of the Higgs potential. Its one-loop flow is given by

$$\beta_t \approx \alpha_t\left[9\alpha_t - \frac{17}{6}\alpha_1 - \frac{9}{2}\alpha_2 - 16\alpha_3\right]. \tag{17}$$

Together with (16) it implies that α_t decreases faster than in the SM. Integrating the flow to leading order in δB_i and to leading logarithmic accuracy, we find

$$\alpha_t(\Lambda) - \alpha_t^{\rm SM}(\Lambda) \approx -\alpha_t(\mu_0)\Delta_t(\mu_0)\ln^2\left(\frac{\Lambda}{\mu_0}\right) < 0,$$
$$\Delta_t = \frac{17}{12}\delta B_1\alpha_1^2 + \frac{9}{4}\delta B_2\alpha_2^2 + 8\delta B_3\alpha_3^2. \tag{18}$$

Note that the result is a resummation effect as (12) and (17) are one loop. One-loop contributions to (18) are absent because the leading-order top running (17) is insensitive to charged new fields, but there is a modification of the one-loop running of gauge couplings contained within (17), which manifests itself at two loop for $\alpha_t(\mu)$.

Turning to the Higgs quartic interaction α_λ, we note that its value is much smaller than the gauge and top Yukawa couplings. Hence, its RGE is primarily driven by the inhomogeneous one-loop terms

$$\beta_\lambda \approx \frac{3}{8}[\alpha_1^2 + 2\alpha_1\alpha_2 + 3\alpha_2^2] - 6\alpha_t^2. \tag{19}$$

We observe that the gauge interactions increase the quartic coupling while the top contribution reduces it. Hence, larger $\alpha_{1,2}$ couplings (16) and a smaller α_t coupling (18) are beneficial for stability. Integrating the flow and subtracting the SM result, and expanding to leading orders in $\delta B_{1,2,3}$ and leading logarithms, we find

$$\alpha_\lambda(\Lambda) - \alpha_\lambda^{\rm SM}(\Lambda) \approx +\frac{3}{8}\alpha_1^2(\mu_0)[\alpha_1(\mu_0) + \alpha_2(\mu_0)]\delta B_1\ln^2\left(\frac{\Lambda}{\mu_0}\right)$$
$$+\frac{3}{8}\alpha_2^2(\mu_0)[\alpha_1(\mu_0) + 3\alpha_2(\mu_0)]\delta B_2\ln^2\left(\frac{\Lambda}{\mu_0}\right)$$
$$+32\alpha_t^2(\mu_0)\alpha_3^2(\mu_0)\delta B_3\ln^3\left(\frac{\Lambda}{\mu_0}\right), \tag{20}$$

which is the central result of this section. A number of comments are in order:

(i) From the result (20) we observe that the enhancement of α_1 and α_2 over SM values (16) also yields a direct uplift of α_λ at two-loop level and leading log, characterized by the terms $\propto \delta B_{1,2}$. There is no such contribution $\propto \delta B_3$ because the Higgs is not charged under $SU(3)_c$.

(ii) The leading impact from the modified running of the strong gauge coupling is channeled through the last term in (19) and therefore suppressed by another loop compared to weak isospin and hypercharge effects. The detour via the top Yukawa implies that the leading contributions $\propto \delta B_3$ to (20) arise at three loop and through leading logs. Quantitatively, the higher-loop suppression may well be compensated by the larger numerical coefficients in the last term of (20) and the size of $\alpha_{3,t}(\mu_0)$. Similar three-loop enhancements via the top coupling also arise $\propto \delta B_{1,2}$, but have not been shown as they are subleading to the terms already in (20).

(iii) Since all terms on the right-hand side of (20) are positive, we conclude that

$$\alpha_\lambda(\Lambda) - \alpha_\lambda^{\rm SM}(\Lambda) > 0, \tag{21}$$

leading to an uplift of the Higgs quartic $\alpha_\lambda(\Lambda)$ and, potentially, stability of the vacuum. The result also establishes that the SM gauge charges (11) of the newly added matter fields all pull into the direction of stability, even though the Higgs does not carry color. We conclude that vectorlike fermions are natural candidates for stability.

(iv) Owing to the fact that the leading loop coefficients of the scalar and top Yukawa beta functions have not changed, the accelerated running of gauge couplings (16) implies that α_λ runs along the SM trajectory but with an accelerated speed, $\alpha_\lambda(\mu) \approx \alpha_\lambda^{\rm SM}(\mu_{\rm SM}(\mu))$ with $\mu_{\rm SM}(\mu) > \mu$. As such, the new α_λ trajectory comes out as a squeezed version of the SM one (Fig. 1), plus a small uplift (21).

(v) A consequence of (21) is that the Higgs quartic, for any gauge portal extension of the SM, is naturally bounded from below by its most negative value achieved in the SM, reading $\alpha_\lambda \gtrsim -10^{-4}$ if we discard the region of the third sign change close to the hypercharge Landau pole.

It is interesting to explore the space of SM extensions with $\delta B_i > 0$ quantitatively. In the remainder, we focus on the strong gauge portal ($\delta B_3 > 0$), the weak gauge portal ($\delta B_2 > 0$), and the hypercharge portal ($\delta B_1 > 0$) separately. We also point out that the strong gauge portal as a mechanism for stability has previously been noted in [68].

B. Strong gauge portal

We study SM extensions with N_F new VLFs in the representation $(0, \mathbf{1}, d_3)$ and of mass M_F, with parameters $\delta B_3 > 0$ and $\delta B_{1,2} = 0$. We refer to the strong gauge portal as the set of parameters N_F, M_F, and d_3, which ensure stability of the vacuum at the Planck scale.

To illustrate the gauge portal mechanism, we consider vectorlike quarks (VLQs) with $d_3 = \mathbf{3}$. We integrate the RG flow up to the Planck scale and take N_F and M_F as free parameters. The UV critical surface of parameters is shown

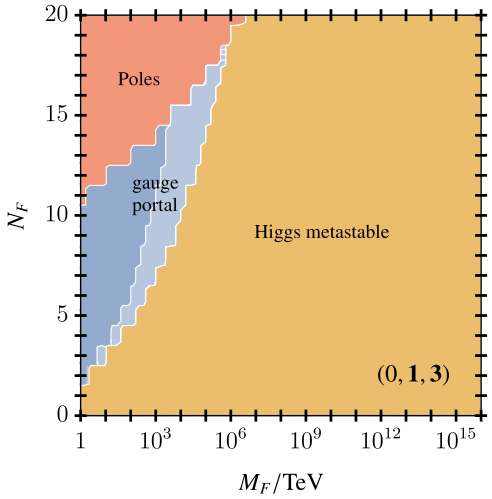

FIG. 2. Illustration of the strong gauge portal for SM extensions with N_F generations of VLQs of mass M_F and in the representation $(0, \mathbf{1}, \mathbf{3})$. Shown is the critical surface in the (N_F, M_F) plane indicating parameter regions where the Higgs potential at the Planck scale remains either metastable such as in the SM (yellow), is plagued by a sub-Planckian Landau pole (red), or has become stable (blue). We further indicate whether the Higgs quartic remains positive along the entire trajectory (dark blue) or whether it has become negative in some range prior to the Planck scale (light blue). We observe that the strong gauge portal opens a wedge that extends moderately into the high mass/high multiplicity region.

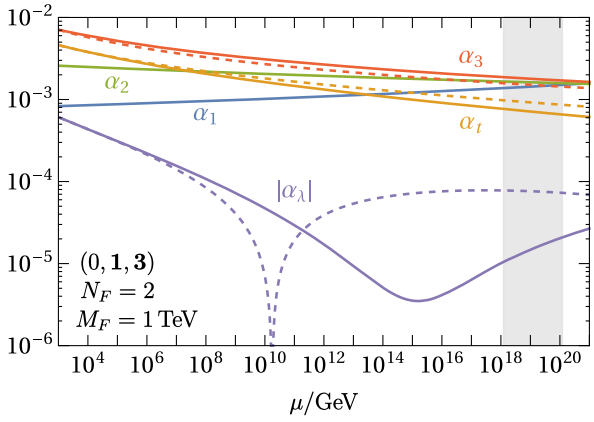

FIG. 3. Example for a strong gauge portal, showing the two-loop running of couplings for a SM extension featuring $N_F = 2$ Dirac fermions (solid lines) in the representation $(0, \mathbf{1}, \mathbf{3})$, in comparison with the SM (dashed lines). The mild enhancement of α_3 together with the mild decrease of α_t ensure that α_λ remains positive throughout.

in Fig. 2, indicating parameter regions where the vacuum at the Planck scale remains metastable (yellow), has become stable (blue), and regions where the RG flow has blown up prior to the Planck scale due to Landau poles (red). We observe that, if M_F is too large and the multiplicity N_F too small, there is not enough "RG time" between M_F and $M_{\rm Pl}$ to lift the potential into stability. The impact is "too little too late," and we are left with metastability of the vacuum just as in the SM (yellow area). On the other hand, if N_F is too large, i.e., $N_F > \frac{21}{2}$, asymptotic freedom in α_3 is lost. If additionally M_F is too small, this may lead to a breakdown of predictivity due to a Landau pole prior to the Planck scale (red area). In particular, this excludes higher representations $d_3 \geq \mathbf{10}$, as a single one of these would cause sub-Planckian Landau poles.

The sweet spot of SM extensions with stable vacua are situated in the wedge (blue regions) between the regions of metastability and Landau poles, characterized by upper and lower bounds on N_F, and an upper bound on M_F. The latter can be understood as follows: For too high values of M_F, SM running implies that $\alpha_{3,t}$ has become too small at the matching scale μ_0 for the uplift (20) to be sufficient. In fact, even if asymptotic freedom is lost, the BSM growth of α_3 and the thereby induced decrease of α_t are insufficient to generate enough uplift (20). We conclude that once $\alpha_t(M_F)$ is too small, the strong gauge portal mechanism is insufficient.

Regions of stability (blue) arise in two manners, either by uplifting the first sign change of α_λ leading to $\alpha_\lambda \geq 0$ for all scales below $M_{\rm Pl}$ (dark blue region) or by pulling the second sign change down to sub-Planckian energies (light blue region). The first case is illustrated in Fig. 3 for $N_F = 2$ and $M_F = 1$ TeV, where the two-loop RG trajectories (solid lines) are contrasted with the SM (dashed lines). We observe that the mild enhancement of α_3 (red) and the mild reduction of the top Yukawa (yellow) over SM running is sufficient to fully stabilize the Higgs quartic (violet), in accord with the analytical estimate in (20).

The second case has settings where the uplift (20) is not enough, but where the squeezing of the α_λ trajectory has pulled down the second sign change to below Planckian energies. Consequently, at the boundary between metastability (yellow) and stability (blue), we find a vanishing quartic at the Planck scale,

$$\lambda|_{\mu=M_{\rm Pl}} = 0. \tag{22}$$

Concrete examples and more details are discussed in Sec. III D (Figs. 7 and 8) below.

Altogether, we observe from Fig. 2 that stability at the Planck scale leads to the parameter constraints

$$\begin{aligned} &M_F \lesssim 10^3 \text{ TeV}, \qquad 2 \leq N_F \leq 14, \\ &(M_F \lesssim 10^6 \text{ TeV}, \qquad 2 \leq N_F \leq 18), \end{aligned} \tag{23}$$

provided we demand stability with $\alpha_\lambda \geq 0$ all the way up to (at least at) the Planck scale. Similar bounds are found for other representations $d_3 < \mathbf{10}$.

The result (23) also demonstrates the constraining power of Planck scale stability. Further, TeV-mass VLQs without or with superfeeble Yukawas to SM fields can be

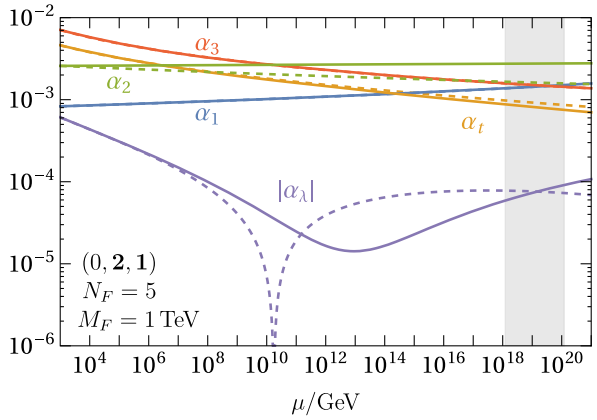

FIG. 4. Example for a weak gauge portal, showing the two-loop running of couplings for a SM extension featuring $N_F = 5$ Dirac fermions (solid lines) in the representation $(0, \mathbf{2}, \mathbf{1})$, in comparison with the SM (dashed lines). The mild enhancement of α_2 ensures that α_λ remains positive throughout.

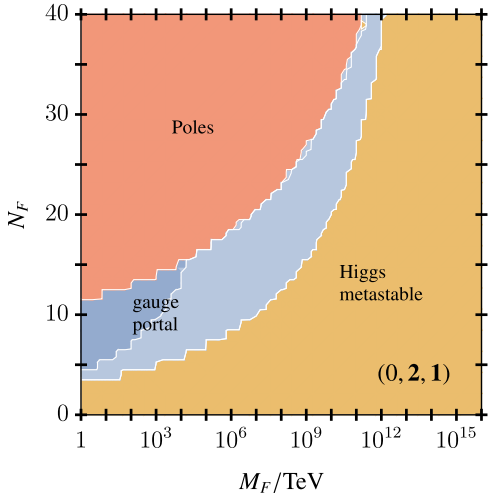

FIG. 5. Illustration of the weak gauge portal for SM extensions with N_F generations of VLLs of mass M_F and in the representation $(0, \mathbf{2}, \mathbf{1})$, showing the critical surface of parameters in the (N_F, M_F) plane with color coding as in Fig. 2. Poles relate to sub-Planckian Landau poles in α_2. We observe that the weak gauge portal extends substantially into the high mass/high multiplicity region.

experimentally probed in R hadron or dijet resonance searches or measurement of α_3 running [90,91].

C. Weak gauge portal

Next, we consider the weak gauge portal characterized by N_F new vectorlike leptons (VLLs) of mass M_F in the representation $(0, d_2, \mathbf{1})$, corresponding to parameters $\delta B_2 > 0$ and $\delta B_{1,3} = 0$. We search for parameter windows where the VLL contributions are sufficiently large to ensure stability of the quartic, but not too large to generate Landau poles in the electroweak couplings below M_{Pl}.

To illustrate the weak gauge portal at work, a concrete example is depicted in Fig. 4 featuring $N_F = 5$ VLLs of mass $M_F = 1$ TeV in the $(0, \mathbf{2}, \mathbf{1})$ representation. We observe that the new VLLs induce a slight enhancement of the weak gauge coupling α_2 (solid green), which proves sufficient to stabilize the Higgs quartic (solid violet curve) along the entire trajectory up to the Planck scale and in accord with the analysis leading up to (20).

The BSM critical surface for SM extensions with N_F VLLs of mass M_F and in the $(0, \mathbf{2}, \mathbf{1})$ representation is shown in Fig. 5. We again observe that the wedge of stability is situated between the metastability and pole regions. Unlike in the strong gauge portal, no upper bound on N_F arises. Consequently, there is no upper limit on M_F either, except at their natural cutoff values around 10^{10} GeV (to stop the sign flip of α_λ) or up to M_{Pl} (otherwise). Larger M_F implies that gauge couplings are much smaller at the matching scale. However, as long as sub-Planckian Landau poles remain absent, this is countered by larger N_F, which allows α_2 to grow fast enough to stabilize the Higgs. We emphasize that this mechanism is not operative for the strong gauge portal.

From Fig. 5 we note that the weak gauge portal starts out at $N_F \geq 5(4)$, depending on whether we demand $\alpha_\lambda \geq 0$ up to (at) the Planck scale. Choosing triplet VLLs $(0, \mathbf{3}, \mathbf{1})$, stability starts for smaller $N_F \geq 2(1)$, and the window is narrower. We also find that $d_2 \geq \mathbf{5}$ leads to sub-Planckian poles already for a single generation.

D. Hypercharge portal

Finally, we consider the hypercharge portal characterized by N_F new VLLs of mass M_F in the representation $(Y_F, \mathbf{1}, \mathbf{1})$, corresponding to parameters $\delta B_1 > 0$ and $\delta B_{2,3} = 0$. Interestingly, also the hypercharge portal is open, despite the looming Landau pole. The BSM critical surface for $Y_F = \frac{1}{2}$ is shown in Fig. 6, where we observe that the stability wedge has a boundary with the metastability region. Most notably, we do not find any region where $\alpha_\lambda > 0$ all the way up to the Planck scale. This states that the uplift in (20) due to hypercharge alone is insufficient.

Instead, stability solely arises through the pull down of the second sign change, which is further illustrated in Fig. 7 for $N_F = 32$ and $Y_F = \frac{1}{2}$. Varying the VLL masses M_F, which corresponds to a horizontal cut across Fig. 6, we observe that the sign changes of α_λ located at trans-Planckian energies in the SM (Fig. 1), are pulled down to below Planckian energies. As such, this illustrates the "squeezing" of the Higgs quartic SM trajectory, see Sec. III A. Evidently, the effect is more pronounced for smaller M_F as this triggers an earlier start of the accelerated α_1 growth. Moreover, if the pull down is too substantial, even the third sign change may arise prior to the Planck scale, typically around $\alpha_1 \gtrsim \text{few} \times 10^{-2}$, followed by a Landau pole shortly thereafter. In consequence, the stability region in Fig. 6

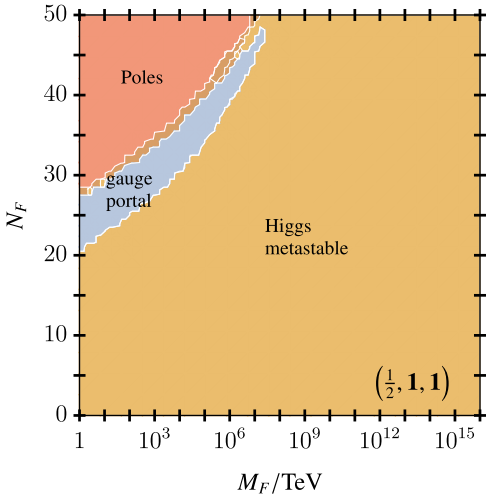

FIG. 6. Illustration of the hypercharge portal for SM extensions with N_F generations of VLLs of mass M_F and in the representation $(\frac{1}{2},\mathbf{1},\mathbf{1})$, showing the critical surface of parameters in the N_F, M_F plane with color coding as in Fig. 2. Here, poles relate to sub-Planckian Landau poles in α_1. We observe that the hypercharge portal extends into the high mass/high multiplicity region. Much unlike the strong and weak gauge portals, we find no regions where the Higgs quartic is positive along the entire trajectory.

develops a border with a new (narrow) region where the vacuum is unstable and just before Landau poles take over. For Fig. 6, we conclude that stability is achievable for $M_F \lesssim 3\times 10^7$ TeV, and $N_F \lesssim 48$.

The hypercharge portal disappears either by increasing M_F, thus leaving insufficient RG time for the pull down to be operative, or by increasing N_F, leading to a third

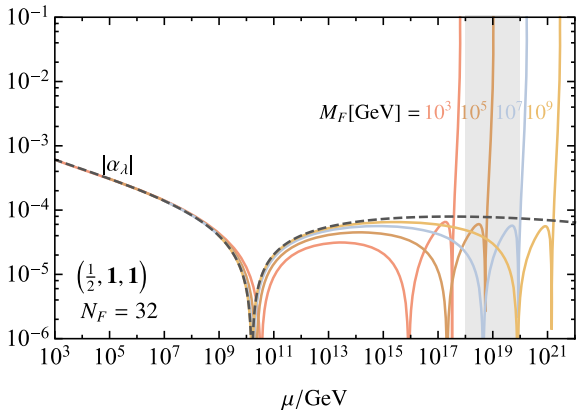

FIG. 7. Example for the "pull down" of sign flips, showing the two-loop running of the Higgs quartic for a SM extension with $N_F = 32$ Dirac fermions in the representation $(\frac{1}{2},\mathbf{1},\mathbf{1})$ for different masses M_F (full lines) in comparison with the SM (dashed line). While the location of the first sign flip is only mildly affected, the location of the second and third ones have moved down significantly from much above the Planck scale (Fig. 1) to the Planckian region and below. The effect is more pronounced for smaller M_F.

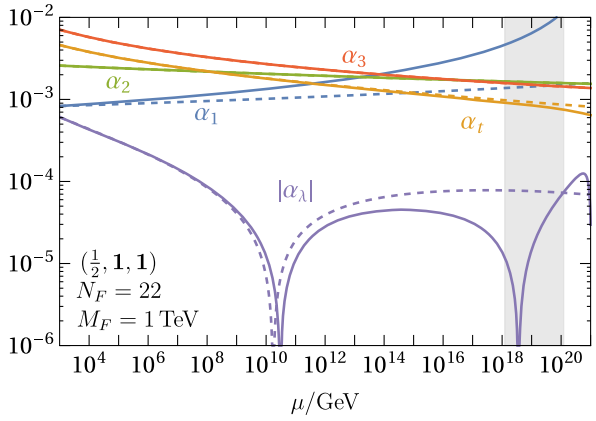

FIG. 8. Example for a hypercharge portal, showing the two-loop running of couplings for a SM extension with $N_F = 22$ Dirac fermions (solid lines) in the representation $(\frac{1}{2},\mathbf{1},\mathbf{1})$ in comparison to the SM (dashed lines). Notice that the enhancement of α_1 has effectively pulled down the second sign change of α_λ in the SM from much above the Planck scale (Fig. 1) to the Planckian region.

sign change or a Landau pole. Similarly, increasing the hypercharge $|Y_F|$ causes the N_F window to become narrower and to move toward lower N_F, and vice versa, reflecting that new terms in the gauge beta functions scale as $\propto N_F Y_F^2$ and $N_F Y_F^4$. Maximal hypercharges are achieved for the smallest number of flavors. We find that, for fixed $M_F = 1$ TeV, $N_F = 6$ flavors achieve stability with $Y_F = 1$. For a single flavor $N_F = 1$, one would need $2.28 < Y_F \leq 2.54$. Increasing the mass for fixed N_F slowly enhances the range of viable hypercharges. For $M_F \simeq 10^{10}$ GeV, the maximal values of Y_F correspond to a narrow window around $Y_F \sim 3.2$–3.3, after which stability can no longer be achieved.

We now turn to a concrete example where the Higgs quartic vanishes identically at Planckian energies. To that end, we exploit the hypercharge portal and tune parameters ($N_F = 22$, $M_F = 1$ TeV, $Y_F = \frac{1}{2}$) appropriately, with results given in Fig. 8. We observe that α_λ changes sign twice, with the second sign flip happening precisely at the Planck scale. We conclude that a vanishing quartic (22) can be achieved at the Planck scale, with the third sign flip still located beyond $M_{\rm Pl}$.

Theory constraints from demanding stability at the Planck scale can be confronted with experimental measurements of the electroweak precision parameters Y and W [92], which depend directly on M_F [93], as well as on N_F via $\delta B_{1,2}$ given in (15). We find that existing constraints for $M_F \gtrsim 1$ TeV are not affecting the weak or hypercharge stability windows. In the absence of Yukawa portals and corresponding decays, LHC searches for long-lived charged particles [94] that leave ionization tracks or $\bar{\psi}\psi$ resonances decaying to diphotons are particularly important. They are available for larger values of electric charge

≥ 1 and $N_F = 1$ and do not exceed ~1 TeV presently. A dedicated analysis of the data and reach of the LHC and future experiments with N_F fermions is desirable but beyond the scope of this work.

E. Higgs criticality

It is interesting to discuss our findings from the viewpoint of Higgs criticality. It has been noticed previously that the SM Higgs quartic approximately obeys $\beta_\lambda|_{\mu=M_{\rm Pl}} \approx 0$ together with $\lambda|_{\mu=M_{\rm Pl}} \approx 0$ to within an accuracy of about $\mathcal{O}(10^{-4})$ [4]. The vanishing of the quartic and its beta function is reminiscent of a free RG fixed point for the quartic.

Given that gauge portals offer mild modifications to the running of the Higgs quartic, it is natural to investigate whether SM extensions can be found where the quartic and its beta function vanish identically. We can answer this question to the affirmative. Specifically, for any gauge portal, α_λ does not change sign (changes sign twice) in the dark blue (light blue) regions of the corresponding critical surface. Therefore, the dark/light blue boundary line corresponds to models where α_λ achieves a double zero at some intermediate scale $M_F \leq \mu_{\rm crit} \leq M_{\rm Pl}$,

$$\lambda|_{\mu_{\rm crit}} = 0 \quad \text{and} \quad \beta_\lambda|_{\mu_{\rm crit}} = 0, \tag{24}$$

corresponding to Higgs criticality at the scale $\mu_{\rm crit}$.

An example for Higgs criticality is shown in Fig. 9, where the strong gauge portal is exploited with two vectorlike quarks in the representation $(0, \mathbf{1}, \mathbf{3})$. For $m_t = 172.76$ GeV, we find that their mass must read $M_F = 1.022$ TeV to achieve (24). In particular, the BSM Higgs quartic remains $\alpha_\lambda \geq 0$ throughout and achieves a double zero $\alpha_\lambda = 0$ just above $\mu_{\rm crit} \approx 10^{15}$ GeV before settling around $\alpha_\lambda \approx 10^{-5}$ at the Planck scale.

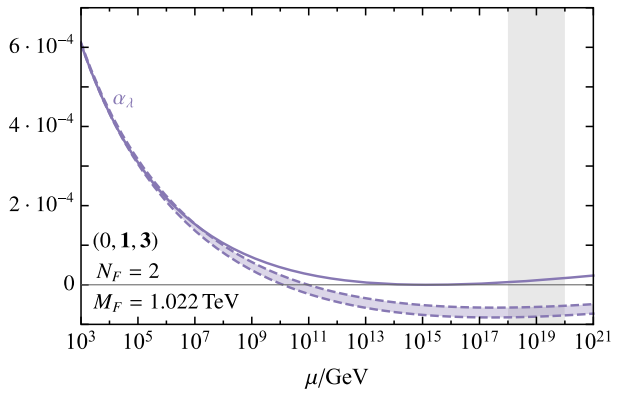

FIG. 9. Higgs criticality in a SM extension with two vectorlike quarks of mass $M_F = 1.022$ TeV. Shown are the running of the BSM Higgs coupling (solid) in comparison to the SM including uncertainties (dashed). We observe that the Higgs quartic develops a double zero at $\mu_{\rm crit} \approx 10^{15}$ GeV and remains positive throughout before settling around $\alpha_\lambda \approx 10^{-5}$ at the Planck scale.

Including the 1σ uncertainty band for the top mass (4) translates into the range $M_F \approx 0.872$–3.767 TeV for the critical mass, where larger M_F relates to lower m_t. As discussed in Sec. III A, the reason why a small uncertainty range in m_t translates into a wide range in M_F is that the value of the top Yukawa has a direct impact on the running of α_λ (19), while the BSM fermions modify α_λ only very indirectly (20).

One may also ask whether the scale for Higgs criticality can be pushed up to the Planck scale,

$$\beta_\lambda|_{\mu=M_{\rm Pl}} = 0, \qquad \lambda|_{\mu=M_{\rm Pl}} = 0. \tag{25}$$

If so, on the critical surface this would have to happen on the intersection of the dark blue/light blue boundary line [where (24) holds true] with the yellow/blue boundary line (where $\alpha_\lambda|_{M_{\rm Pl}} = 0$ holds true). This is where (22) and (24) are valid simultaneously, and the scale $\mu_{\rm crit}$ in (22) then coincides with the Planck scale. For this to happen, we need the two sign changes of α_λ in the SM to coincide at the Planck scale. From our model studies, we observe that the strong and weak gauge portals can achieve sufficient uplift for that, Figs. 2 and 5, but the scale of criticality comes out in the region

$$\mu_{\rm crit} \approx 10^{11} - 10^{15}\ \text{GeV}, \tag{26}$$

a few orders of magnitude below $M_{\rm Pl}$. The hypercharge portal on its own cannot achieve enough uplift, Fig. 6, and criticality is out of reach.

Finally, we emphasize that models with Higgs criticality around (26) lead to $\beta_\lambda|_{\mu=M_{\rm Pl}} \approx 0$ together with $\lambda|_{\mu=M_{\rm Pl}} \approx 0$ and to an accuracy similar or lower than observed in the SM (see Fig. 9). Future work should clarify whether more sophisticated gauge portals can push the scale of criticality fully up to the Planck scale.

IV. GAUGE-YUKAWA PORTALS

In this section, we consider SM extensions with vectorlike fermions $\psi_{L,R}$ in representations that allow for renormalizable Yukawa interactions with SM and BSM fermions and the Higgs. Thirteen different types of SM extensions exist, given in Table I, featuring vectorlike leptons (models A–F) or vectorlike quarks (models G–M).

The presence of Yukawa interactions modifies the RG running and may impact both the position of Landau poles and the stability of the Higgs potential. Generically, Landau poles in the gauge sector are moved toward higher scales, but the extent of the shift depends on fermion representations, as well as the structure and strength of the Yukawa portal. Similarly, estimating the effects on vacuum stability requires a dedicated study for each of the models in Table I.

We begin investigating the models in the limit of feebly small Yukawa portals in Sec. IV A. Next, we conduct a stability analysis for Yukawas to the third generation of SM fermions in Sec. IV B. In Sec. IV C, we detail the running

TABLE I. Complete list of vectorlike fermion extensions of the SM with Yukawa portals to the Higgs and SM fermions, also showing the respective gauge charges and interactions; $H^c = i\sigma_2 H^*$. Note that model K offers two Yukawa portals.

Model	(Y_F, d_2, d_3)	Yukawa interactions
A	$(-1, \mathbf{1}, \mathbf{1})$	$\kappa_{ij}\bar{L}_i H \psi_{Rj} + \text{h.c.}$
B	$(-1, \mathbf{3}, \mathbf{1})$	$\kappa_{ij}\bar{L}_i \psi_{Rj} H + \text{h.c.}$
C	$\left(-\frac{1}{2}, \mathbf{2}, \mathbf{1}\right)$	$\kappa_{ij}\bar{\psi}_{Li} H E_j + \text{h.c.}$
D	$\left(-\frac{3}{2}, \mathbf{2}, \mathbf{1}\right)$	$\kappa_{ij}\bar{\psi}_{Li} H^c E_j + \text{h.c.}$
E	$(0, \mathbf{1}, \mathbf{1})$	$\kappa_{ij}\bar{L}_i H^c \psi_{Rj} + \text{h.c.}$
F	$(0, \mathbf{3}, \mathbf{1})$	$\kappa_{ij}\bar{L}_i \psi_{Rj} H^c + \text{h.c.}$
G	$\left(-\frac{1}{3}, \mathbf{1}, \mathbf{3}\right)$	$\kappa_{ij}\bar{Q}_i H \psi_{Rj} + \text{h.c.}$
H	$\left(+\frac{2}{3}, \mathbf{1}, \mathbf{3}\right)$	$\kappa_{ij}\bar{Q}_i H^c \psi_{Rj} + \text{h.c.}$
I	$\left(-\frac{1}{3}, \mathbf{3}, \mathbf{3}\right)$	$\kappa_{ij}\bar{Q}_i \psi_{Rj} H + \text{h.c.}$
J	$\left(+\frac{2}{3}, \mathbf{3}, \mathbf{3}\right)$	$\kappa_{ij}\bar{Q}_i \psi_{Rj} H^c + \text{h.c.}$
K	$\left(+\frac{1}{6}, \mathbf{2}, \mathbf{3}\right)$	$\kappa^u_{ij}\bar{\psi}_{Li} H^c U_j + \kappa^d_{ij}\bar{\psi}_{Li} H D_j + \text{h.c.}$
L	$\left(+\frac{7}{6}, \mathbf{2}, \mathbf{3}\right)$	$\kappa_{ij}\bar{\psi}_{Li} H U_j + \text{h.c.}$
M	$\left(-\frac{5}{6}, \mathbf{2}, \mathbf{3}\right)$	$\kappa_{ij}\bar{\psi}_{Li} H^c D_j + \text{h.c.}$

and walking windows in VLQ models, before turning to flavorful models in Sec. IV D.

A. Feeble Yukawas and gauge portals

Yukawa portals from vectorlike fermions to the Higgs are technically natural and can hence be made feebly small, or even vanishing. In this limit, the vacuum stability is controlled by the gauge portal (Sec. III).

For $M_F \simeq 1$ TeV, stability constraints on N_F for the various models A–M are collected in Table II. We observe that models E, I, J, and L do not achieve a stable vacuum at the Planck scale, not even with a single BSM generation. For model E this is trivially so because it does not exhibit a gauge portal as the BSM fermions are singlets, hence SM metastability prevails. Models I, J (and L) are afflicted by sub-Planckian Landau poles in α_2 (α_1), which can be remedied provided the new fields have larger masses ($M_F \gg$ TeV), whereby viable gauge portals open up (we demonstrate this explicitly for model L in Fig. 14). Vectorlike lepton models A–D and F have a finite range of stability in N_F. Models are constrained by Landau poles in $\alpha_{1,2}$. Note that, since the representations in E and F are real, an odd number of BSM Weyl fermions is compatible with gauge anomaly cancellation, corresponding to half-integer values of N_F. Finally, for suitable values of N_F, for vectorlike quark models G, H, K, M, and $M_F = 1$ TeV, we find that $\alpha_\lambda \geq 0$ all the way up to the Planck scale.

Keeping both N_F and M_F as free parameters, the critical surface is exemplarily shown for model G in Fig. 10. We observe that a wedge of stability arises between regions of metastability and Landau poles, bounded by upper and lower limits on N_F and an upper limit on M_F. Similar results are found for models B, C, F, H, and K (not shown).

TABLE II. Planck scale stability of SM extensions as in Table I for $M_F = 1$ TeV and vanishing Yukawa portal couplings $\alpha_\kappa|_{1\text{ TeV}} \simeq 0$. Parameter regions indicate stability at the Planck scale ($\alpha_\lambda|_{M_{\rm Pl}} \geq 0$), stability for all scales up to $M_{\rm Pl}$ ($\alpha_\lambda \geq 0$), and the type of singularity above the upper end of stability. Model E remains metastable as the SM, and models I, J, and L display Landau poles prior to $M_{\rm Pl}$.

Model	Poles		Stability	
(Y_F, d_2, d_3)	$N_F^{\rm pole}$	$\alpha^{\rm pole}$	$\alpha_\lambda|_{M_{\rm Pl}} \geq 0$	$\alpha_\lambda \geq 0$
A $(-1, \mathbf{1}, \mathbf{1})$	7	α_1	$N_F = 6$	X
B $(-1, \mathbf{3}, \mathbf{1})$	3	α_1	$1 \leq N_F \leq 2$	$1 \leq N_F \leq 2$
C $\left(-\frac{1}{2}, \mathbf{2}, \mathbf{1}\right)$	12	α_2	$3 \leq N_F \leq 11$	$5 \leq N_F \leq 11$
D $\left(-\frac{3}{2}, \mathbf{2}, \mathbf{1}\right)$	2	α_1	$N_F = 1$	X
E $(0, \mathbf{1}, \mathbf{1})$	As in SM		X	X
F $(0, \mathbf{3}, \mathbf{1})$	3	α_2	$1 \leq N_F \leq \frac{5}{2}$	$\frac{3}{2} \leq N_F \leq \frac{5}{2}$
G $\left(-\frac{1}{3}, \mathbf{1}, \mathbf{3}\right)$	11	α_3	$2 \leq N_F \leq 10$	$2 \leq N_F \leq 10$
H $\left(+\frac{2}{3}, \mathbf{1}, \mathbf{3}\right)$	6	α_1	$2 \leq N_F \leq 5$	$2 \leq N_F \leq 5$
I $\left(-\frac{1}{3}, \mathbf{3}, \mathbf{3}\right)$	1	α_2	X	X
J $\left(+\frac{2}{3}, \mathbf{3}, \mathbf{3}\right)$	1	α_2	X	X
K $\left(+\frac{1}{6}, \mathbf{2}, \mathbf{3}\right)$	4	α_2	$1 \leq N_F \leq 3$	$1 \leq N_F \leq 3$
L $\left(+\frac{7}{6}, \mathbf{2}, \mathbf{3}\right)$	1	α_1	X	X
M $\left(-\frac{5}{6}, \mathbf{2}, \mathbf{3}\right)$	2	α_1	$N_F = 1$	$N_F = 1$

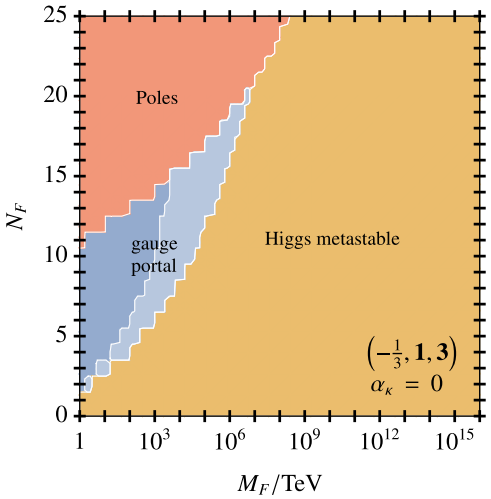

FIG. 10. Illustration of a gauge portal for stability from strong gauge and hypercharge contributions (model G with $\alpha_\kappa = 0$), showing the critical surface of parameters in the (N_F, M_F) plane with color coding as in Fig. 2. The pole region relates to sub-Planckian Landau poles in α_3.

TABLE III. Vacuum stability at the Planck scale for SM extensions with a single vectorlike fermion of mass $M_F = 1$ TeV and Yukawa couplings to the Higgs and third-generation SM fermions. Shown are the parameter ranges of Yukawa couplings at the matching scale ($\mu_0 = M_F$) which ensure stability via either the gauge or the Yukawa portal. Values without (with) brackets refer to settings where $\alpha_\lambda \geq 0$ ($\alpha_\lambda|_{M_{\rm Pl}} \geq 0$). For small $\alpha_\kappa(\mu_0)$, we observe that a few models offer stability via a gauge portal. For moderate or large $\alpha_\kappa(\mu_0)$, stability is provided by the Yukawa portal and a strongly coupled walking regime. For vanishing Yukawas, the results of Table II are recovered.

Model	(Y_F, d_2, d_3)	Interactions	Gauge portal	Yukawa portal
A	$(-1, \mathbf{1}, \mathbf{1})$	$\kappa \bar{L}_3 H \psi_R$	X	$\alpha_\kappa\|_{1\ \mathrm{TeV}} \gtrsim 0.20 (6 \times 10^{-3})$
B	$(-1, \mathbf{3}, \mathbf{1})$	$\kappa \bar{L}_3 \psi_R H$	$\alpha_\kappa\|_{1\ \mathrm{TeV}} \lesssim 2 \times 10^{-4} (1.6 \times 10^{-3})$	$\alpha_\kappa\|_{1\ \mathrm{TeV}} \gtrsim 0.4 (1.6 \times 10^{-2})$
C	$\left(-\frac{1}{2}, \mathbf{2}, \mathbf{1}\right)$	$\kappa \bar{\psi}_L H E_3$	X	$\alpha_\kappa\|_{1\ \mathrm{TeV}} \gtrsim 0.20 (6 \times 10^{-3})$
D	$\left(-\frac{3}{2}, \mathbf{2}, \mathbf{1}\right)$	$\kappa \bar{\psi}_L H^c E_3$	$(\alpha_\kappa\|_{1\ \mathrm{TeV}} \lesssim 3 \times 10^{-5})$	$\alpha_\kappa\|_{1\ \mathrm{TeV}} \gtrsim 0.20 (8 \times 10^{-3})$
E	$(0, \mathbf{1}, \mathbf{1})$	$\kappa \bar{L}_3 H^c \psi_R$	X	$\alpha_\kappa\|_{1\ \mathrm{TeV}} \gtrsim 0.20 (5 \times 10^{-3})$
F	$(0, \mathbf{3}, \mathbf{1})$	$\kappa \bar{L}_3 \psi_R H^c$	$(\alpha_\kappa\|_{1\ \mathrm{TeV}} \lesssim 10^{-3})$	$\alpha_\kappa\|_{1\ \mathrm{TeV}} \gtrsim 0.4 (1.6 \times 10^{-2})$
G	$\left(-\frac{1}{3}, \mathbf{1}, \mathbf{3}\right)$	$\kappa \bar{Q}_3 H \psi_R$	X	$\alpha_\kappa\|_{1\ \mathrm{TeV}} \gtrsim 0.20 (1 \times 10^{-2})$
H	$\left(+\frac{2}{3}, \mathbf{1}, \mathbf{3}\right)$	$\kappa \bar{Q}_3 H^c \psi_R$	X	$\alpha_\kappa\|_{1\ \mathrm{TeV}} \gtrsim 0.20 (6 \times 10^{-3})$
I	$\left(-\frac{1}{3}, \mathbf{3}, \mathbf{3}\right)$	$\kappa \bar{Q}_3 \psi_R H$	X	$\alpha_\kappa\|_{1\ \mathrm{TeV}} \gtrsim 0.6 (0.3)$
J	$\left(+\frac{2}{3}, \mathbf{3}, \mathbf{3}\right)$	$\kappa \bar{Q}_3 \psi_R H^c$	X	$\alpha_\kappa\|_{1\ \mathrm{TeV}} \gtrsim 0.6 (0.3)$
K	$\left(+\frac{1}{6}, \mathbf{2}, \mathbf{3}\right)$	$\kappa_t \bar{\psi}_L H^c U_3 + \kappa_b \bar{\psi}_L H D_3$	$\alpha_{\kappa_t, \kappa_b(\kappa_t)}\|_{1\ \mathrm{TeV}} \lesssim 10^{-5} (10^{-4})$	$\alpha_{\kappa_t, \kappa_b}\|_{1\ \mathrm{TeV}} \gtrsim 0.25 (0.13)$
L	$\left(+\frac{7}{6}, \mathbf{2}, \mathbf{3}\right)$	$\kappa \bar{\psi}_L H U_3$	X	$\alpha_\kappa\|_{1\ \mathrm{TeV}} \gtrsim 0.20 (10^{-2})$
M	$\left(-\frac{5}{6}, \mathbf{2}, \mathbf{3}\right)$	$\kappa \bar{\psi}_L H^c D_3$	$\alpha_\kappa\|_{1\ \mathrm{TeV}} \lesssim 8 \times 10^{-4} (1.4 \times 10^{-3})$	$\alpha_\kappa\|_{1\ \mathrm{TeV}} \gtrsim 0.2 (8 \times 10^{-3})$

B. Third-generation Yukawa portals

In this section, we study the impact of Yukawa portals. We consider the SM extensions given in Table I (models A–M) taking $M_F = 1$ TeV and a minimal number of BSM fermions, $N_F = 1$. For simplicity, we only retain a single Yukawa κ (there are two in model K), coupling to third-generation SM fermions. This is in accord with the flavor symmetry implications of (2).

We then integrate the running couplings up to the Planck scale and perform a scan by using the BSM Yukawa coupling $\alpha_\kappa|_{M_F}$ as a free parameter to find conditions for vacuum stability. Our main findings are compiled in Table III. For feeble Yukawas, models display diverse phenomena such as stability with $\alpha_\lambda \geq 0$ (models B, K, M) or with $\alpha_\lambda|_{M_{\rm Pl}} \geq 0$ (models D, F), Higgs metastability at the Planck scale (models A, C, E, G, H), or sub-Planckian Landau poles (models I, J, L). We further observe that all models that achieve stability through a gauge portal for vanishing Yukawa interactions, Table II, continue to do so up to a small upper limit for the Yukawa coupling α_κ (models B, D, F, K, and M). This is in accord with expectations from perturbation theory, which showed that small Yukawa interactions counteract stability, (7).

By the same token, away from feeble or weak-sized values, Yukawa portal interactions destabilize the Higgs potential, and we find that stability cannot be achieved for a range of Yukawa couplings. However, a new effect sets in for moderate or larger Yukawa couplings, which trigger a walking regime whereby couplings are almost interlocked due to the proximity of a partial fixed point. Incidentally, this effect helps stabilize both the running of the scalar coupling as well as preventing sub-Planckian Landau poles [74,81]. In consequence, a new window into Higgs stability opens up to which we refer as the Yukawa portal. We note that Yukawa portals are available for all models including for those without viable gauge portals for small Yukawas. The onset for this can happen for Yukawas as low as $\alpha_\kappa \gtrsim 5 \times 10^{-3}$, depending on the model, though for some models the onset is borderline nonperturbative ($\alpha_\kappa \gtrsim 0.3$). Upper bounds on stability are dictated by the loss of perturbative control. Regions of stability are illustrated in Fig. 11 (model M).

We note that stability is largely insensitive to our choice of connecting the Yukawa portal to the third generation, as mixed terms in beta functions containing both SM and BSM Yukawas are numerically small with very little impact on the running. The reason we selected the third generation of SM fermions is that their BSM search window is larger. We discuss phenomenological constraints in Sec. IV E.

C. Running and walking

To further appreciate the different mechanisms for stability as indicated in Table III, we investigate the RG running of α_λ in dependence of $\alpha_\kappa(\mu_0)$ in more detail for model M (Fig. 11).

Figure 12 shows the running of α_λ between $\mu_0 = 1$ TeV and the Planck scale for selected values of α_κ at the matching scale μ_0. For any α_κ, we find a Landau pole in the trans-Planckian regime $\mu \simeq 5 \times 10^{23}$ GeV owing to the

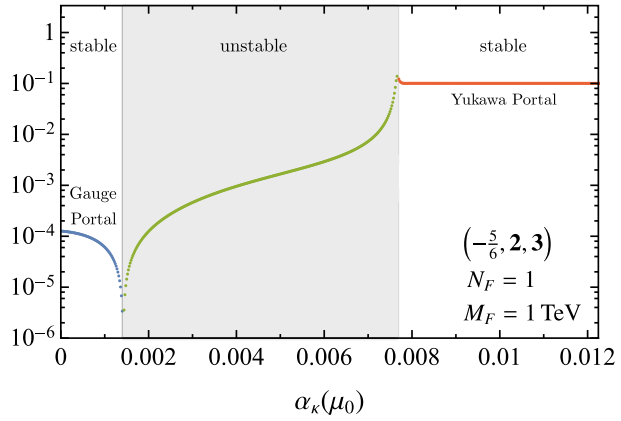

FIG. 11. Shown is the Higgs quartic coupling at the Planck scale $|\alpha_\lambda(M_{\rm Pl})|$ as a function of the Yukawa portal coupling α_κ (model M, $N_F = 1$, $M_F = 1$ TeV). Stability is achieved through the gauge portal (blue) or the Yukawa portal (red). In between, stability cannot be achieved (green).

hypercharge. For sufficiently small $\alpha_\kappa \lesssim 8 \times 10^{-4}$ (dark blue, violet), the gauge portal is operative leading to stability $\alpha_\lambda \geq 0$ along the entire trajectory. We observe that α_λ exhibits a minimum around $\mu_{\rm min} \approx 10^{13}$ GeV where the value of $\alpha_\lambda(\mu_{\rm min})$ decreases with increasing α_κ. Within the range $8 \times 10^{-4} \lesssim \alpha_\kappa \lesssim 1.4 \times 10^{-3}$ illustrated by the light blue curve, the running α_λ becomes mildly negative for a range of scales, but stability prevails in the end $[\alpha_\lambda(M_{\rm Pl}) \geq 0]$. The width of the metastability regime quickly increases with growing α_κ until the second zero occurs at the Planck scale ($\alpha_\kappa \simeq 1.4 \times 10^{-3}$) implying a flat potential (22). Increasing α_κ even further pushes this second sign flip beyond the Planck scale and stability is lost (green) for a range of α_κ.

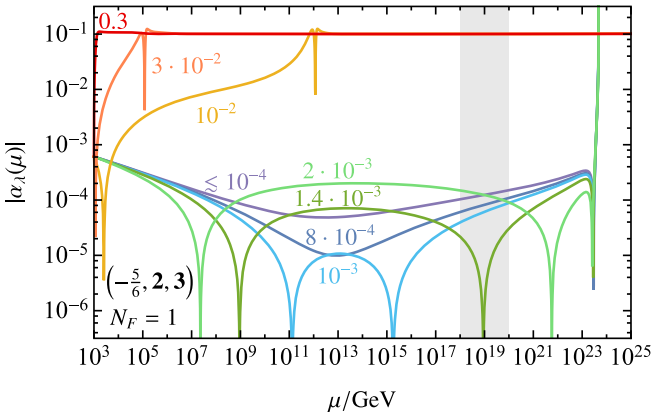

FIG. 12. Shown is the transition from the gauge to the Yukawa portal (model M, $N_F = 1$, $M_F = 1$ TeV) by varying the Yukawa coupling $\alpha_\kappa|_{M_F}$ between 10^{-4} and 3×10^{-1}. For feeble α_κ (violet) the Higgs potential is stabilized by the gauge portal. Increasing α_κ generates two sign flips for α_λ (blue), one of which moves beyond $M_{\rm Pl}$ to destabilize the vacuum (green). For α_κ beyond 10^{-2} (yellow, orange, red), the Higgs is stabilized through a strongly coupled Yukawa portal.

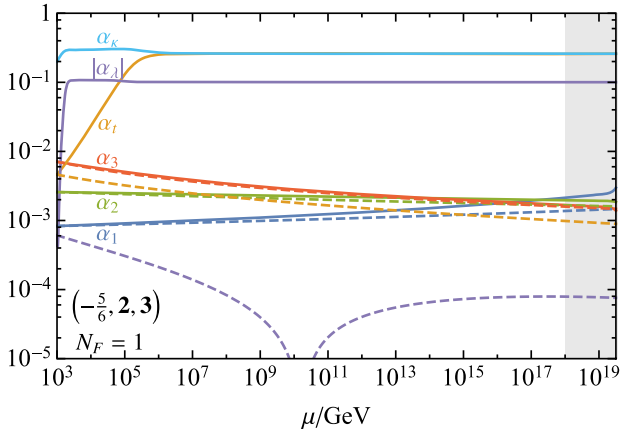

FIG. 13. Example of a Yukawa portal, showing the two-loop running of couplings in model M of Table III (SM plus a VLF of mass 1 TeV and BSM Yukawa coupling α_κ). The RG flow is depicted for large initial $\alpha_\kappa|_{\mu_0 = M_F} = 0.2$. We observe a walking regime for the Yukawa and quartic couplings $\alpha_{\kappa,t,\lambda}$ at sizable values, while the gauge couplings continue to evolve within a weakly coupled regime all the way up to the Planck scale, similar to their running in the SM (dashed).

A new effect sets in when $\alpha_\kappa \simeq 8 \times 10^{-3}$. While we observe a region of instability starting above 1 TeV, the Higgs coupling is subsequently pulled up to positive values (yellow and orange curves) and achieves stability with $\alpha_\lambda(M_{\rm Pl}) \approx 0.1$. Since the quartic and Yukawa couplings run very slowly, we refer to this as the "walking regime" (see footnote 1). The larger α_κ, the earlier α_λ enters into a walking regime. For large $\alpha_\kappa \gtrsim 0.2$, the walking regime starts straight after the matching scale and we have $\alpha_\lambda \geq 0$ along the entire trajectory.

The latter result can also be inferred from Fig. 13 where the running of couplings (with $\alpha_\kappa = 0.2$) is displayed (full lines) and compared with the SM (dashed lines). We observe that the Higgs, the top, and the BSM Yukawa couplings run very slowly, while gauge couplings continue to evolve as in the SM.[3]

Next, we study the impact of the BSM mass scale M_F on the RG fate of two complementary VLQ models: Model M has stability windows from the gauge and the Yukawa portal, while model L only features stability from the latter. The RG anatomy of VLL models has been the subject of [74]. The critical surface spanned by M_F and $\alpha_\kappa(M_F)$ is displayed in Fig. 14 for model M (upper plot) and model L (lower plot).

For model M, we find that stability is achieved via the gauge portal for masses up to $M_F \approx 3 \times 10^3$ TeV and for Yukawas up to $\alpha_\kappa(M_F) \approx 10^{-3}$. Increasing M_F further leads to metastability. Increasing $\alpha_\kappa(M_F)$ we find a narrow band of instability, for any M_F, after which the Yukawa portal opens

[3]Neglecting contributions from $\alpha_{1,b,\lambda}$, we find that the BSM and top Yukawa beta functions are identical after exchanging $\alpha_\kappa \leftrightarrow \alpha_t$. This explains why α_κ and α_t asymptote to nearby values.

up. The latter extends up to $M_F \simeq 10^7$ TeV if we demand stability along the entire trajectory, $\alpha_\lambda \geq 0$. Interestingly, the upper limit on the VLF mass coincides with the scale where the Higgs quartic flips sign in the SM, which is the natural upper limit. Similarly, if we demand stability at the Planck scale $\alpha_\lambda|_{M_{\rm Pl}} \geq 0$, we find stability in a more substantial range up to $M_F \simeq 10^{16}$ TeV, in accord with Table III.

In contrast, model L does not offer a gauge portal for small M_F and small α_κ. However, a gauge portal opens up in the range $3\times10^2 \lesssim M_F \lesssim 10^6$ TeV for small $\alpha_\kappa(M_F) \lesssim 3\times10^{-4}$. The reason for this is that the Landau pole at $\mu \simeq 10^{14}$ TeV, which arises for low $M_F \approx 1$ TeV, is pushed beyond the Planck scale by increasing M_F by 2 orders of magnitude, and stability is achieved $\alpha_\lambda|_{M_{\rm Pl}} \geq 0$. For larger masses, the potential becomes metastable, much like in model M. Also, increasing $\alpha_\kappa(M_F)$ leads to a narrow band of instability, for any M_F, after which the Yukawa portal opens up, which quantitatively is very similar to the one found in model M.

D. Flavorful Yukawas

In this section, we generalize the SM extensions from Sec. IV B by allowing for Yukawa couplings to all three generations of SM fermions, while keeping $N_F = 1$ BSM fermions. This accounts for all renormalizable portal interactions compatible with symmetries, rendering portal couplings $\vec{\kappa}$ a vector in the SM generations. The approximation (2) implies that the non-Abelian flavor symmetry

$$U(2)_Q \times U(2)_U \times U(2)_D \times U(3)_L \times U(3)_E \quad (27)$$

is retained for SM leptons as well as the first and second quark generations. Hence, a suitable ansatz for the portal couplings reads

$$\vec{\kappa} = \begin{cases} (\kappa,\kappa,\kappa)^\intercal & \text{for VLLs} \\ (\kappa,\kappa,\tilde{\kappa})^\intercal & \text{for VLQs} \end{cases}, \quad (28)$$

featuring a universal coupling to parametrize the portal in VLL models, and κ and $\tilde{\kappa}$ for VLQs.

Changing from single coupling $\vec{\kappa} = (0,0,\kappa)$ discussed in Sec. IV B to triple (28) has minor qualitative impact on the BSM critical surfaces. The only notable difference for VLL models (A–F) is a shift by roughly half an order of magnitude toward lower values of $\alpha_\kappa(M_F)$ compared to the single Yukawa case. The origin for this minor modification is that contributions to the β functions from fermion bubble diagrams involving α_κ pick up an additional factor of 3 compared to the single Yukawa case.

For VLQs, on the other hand, with (28) two independent Yukawa couplings $\alpha_{\kappa,\tilde{\kappa}}$ are present. A section of the BSM critical surface with $\alpha_\kappa(M_F) = \alpha_{\tilde{\kappa}}(M_F)$ versus M_F is displayed in the bottom panels of Figs. 15 and 16 for models M and L, respectively. One notes a strong resemblance to Fig. 14 in the single Yukawa case up to a factor $\lesssim$3 shift toward lower values of $\alpha_\kappa(M_F)$.

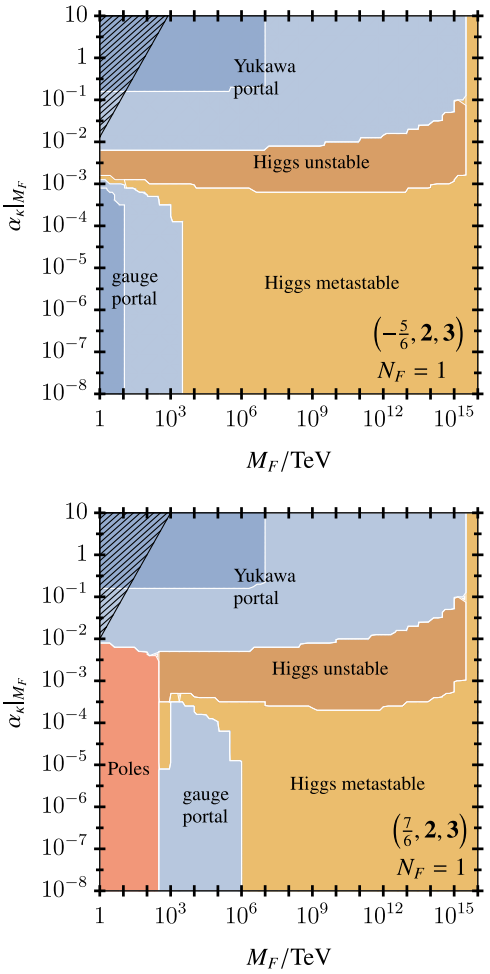

FIG. 14. Critical surfaces in the M_F and $\alpha_\kappa|_{M_F}$ plane for model M (top) and L (bottom) for $N_F = 1$; color coding as in Fig. 2, also indicating unstable potentials $\alpha_\lambda < -10^{-4}$ (brown). Standard Model effective field theory (SMEFT) 90% confidence level (CL) exclusion regions on α_κ/M_F^2 [95,96] are indicated by the black hatched regions.

The upper panels of Figs. 15 and 16 display $\alpha_\kappa(M_F)$ versus $\alpha_{\tilde{\kappa}}(M_F)$ for $M_F = 1$ TeV. For sufficiently small $\alpha_\kappa(M_F)$ the stability conditions are consistent with Table III. Moreover, the surface plot is basically symmetric under interchange $\alpha_\kappa \leftrightarrow 2\alpha_{\tilde{\kappa}}$. This reflects the finding from Sec. IV B that the RG evolution is essentially unchanged if the VLF couples to a first- or second- instead of third-generation SM fermion, as mixed SM-BSM Yukawa contributions to the RGEs are numerically small and of minor importance.

While the impact of a larger Yukawa portal is qualitatively minor for stability, it is important for phenomenology, discussed in the next section.

E. Mass limits

We briefly comment on experimental probes of VLF models. In the presence of the Yukawa portal that induces

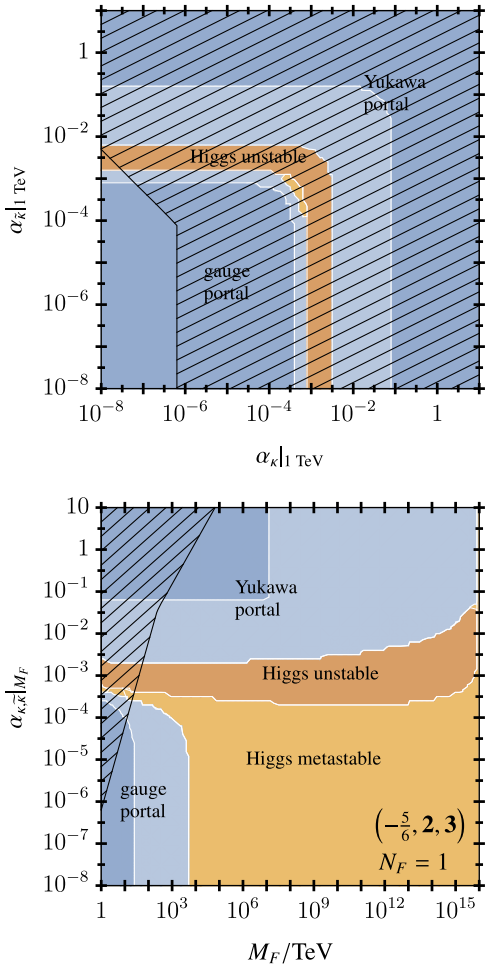

FIG. 15. BSM critical surface for model M with $N_F = 1$ and Yukawa couplings to all SM fermion generations (28) scanning over $\alpha_{\kappa,\tilde{\kappa}}|_{1\text{ TeV}}$ (top) as well as M_F and $\alpha_\kappa|_{M_F} = \alpha_{\tilde{\kappa}}|_{M_F}$ (bottom); color coding as in Figs. 2 and 14. Regions excluded by $\Delta F = 1$ or $\Delta F = 2$ FCNC bounds on α_κ/M_F^2 and α_κ^2/M_F^2, respectively, are indicated by the black hatched areas. Most stringent constraints are from $K_L \to \mu\mu$ decays and K mixing [97].

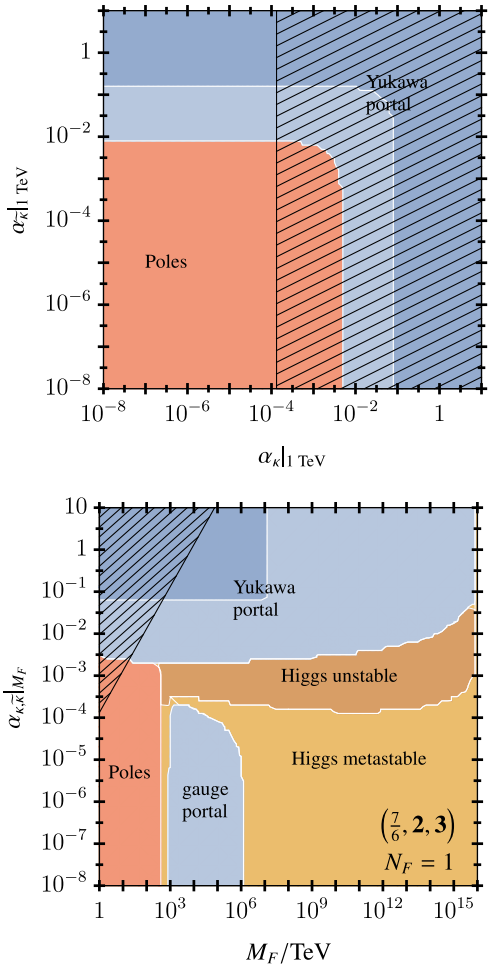

FIG. 16. BSM critical surface as in Fig. 15 for model L with $N_F = 1$ and Yukawa couplings to all three SM fermion generations scanning over $\alpha_{\kappa,\tilde{\kappa}}|_{1\text{ TeV}}$ (top) as well as M_F and $\alpha_\kappa|_{M_F} = \alpha_{\tilde{\kappa}}|_{M_F}$ (bottom); color coding as in Figs. 2 and 14. The most stringent FCNC bound is from one-loop contributions to D mixing [97].

VLF decay, pair and single production searches (e.g., [98,99]) can be used to constrain M_F and α_κ/M_F^2, respectively. In addition, global SMEFT fits allow one to constrain α_κ/M_F^2, too. A detailed analysis of constraints is given elsewhere [97,100,101]. Here we show that stability requirements and experimental constraints are complementary and allow one to obtain new limits on the BSM masses. In particular, collider and flavor measurements are probing the walking regime with large Yukawas, i.e., the Yukawa portal at work.

We discuss the theory-collider interplay in the case of model L, beginning with the third-generation only scenario: The SMEFT exclusion region on $\alpha_\kappa/M_F^2 < 0.01\ \text{TeV}^{-2}$ at 90% CL from a single operator fit [96] is indicated by the black hatched region in the lower plot of Fig. 14. There exists also a lower limit $M_F > 1.37$ TeV at 95% CL from pair production from ATLAS [98] for this model, not shown for clarity. Combining the stability constraints with the experimental limits yields the allowed mass windows

$$4\ \text{TeV} \lesssim M_F \lesssim 10^7\ \text{TeV}$$
$$(1\ \text{TeV} \lesssim M_F \lesssim 10^{16}\ \text{TeV}), \tag{29}$$

for $\alpha_\lambda \geq 0$ up to the Planck scale (at the Planck scale). The lower limits are stronger than (similar to) the ones from direct searches.

Experimentally, flavorful Yukawa portal couplings (28) are severely constrained by flavor-changing neutral current (FCNC) processes. These are generically induced at tree level from Z penguins via fermion mixing and from Higgs-VLF loops. These bounds are typically orders of magnitude stronger than the single Yukawa ones, such as (29). For instance, in model L, combining Higgs stability conditions with FCNC exclusion limits from D mixing [97],

$\alpha_\kappa/M_F \lesssim 1.3 \times 10^{-4}$ TeV^{-1}, yields in the flavor universal benchmark $\alpha_\kappa(\mu_0) = \alpha_{\tilde{\kappa}}(\mu_0)$ the limits

$$480\,\text{TeV} \lesssim M_F \lesssim 10^7\ \text{TeV}$$
$$(19\,\text{TeV} \lesssim M_F \lesssim 10^{16}\ \text{TeV}), \tag{30}$$

which can be read off from Fig. 16. The lower limits are significantly stronger than those in (29) and existing collider search limits. The stronger (weaker) limits refer to $\alpha_\lambda \geq 0$ up to the Planck scale (at the Planck scale).

All models A–M exhibit a very similar pattern of regions (poles, stability, metastability) in the α_κ–M_F surface plots. As exemplified by Fig. 14, the main difference is in the lower left corner, covering a low-scale gauge portal with feeble Yukawas and masses in the (multi-)TeV range. Models that do not feature stability here, such as model L, but also VLQs I and J are subject to BSM mass constraints from a combination of experimental searches and stability as in (29) and (30). For the other models, such as model M, no lower mass limit can be obtained from our analysis. Furthermore, if the Yukawa portal is too small or vanishes, collider searches for long-lived particles become important. Long-lived charged particles [94] leave ionization tracks or form resonances that decay to photons. Long-lived VLQs in addition lead to R hadron or dijet resonance signatures [91].

For VLLs, mass bounds are even stronger than (30) as charged lepton flavor violation is experimentally more severely constrained than FCNCs in the quark sector. In particular, results from μ–e-conversion experiments [97] yield bounds as strong as $M_F \gtrsim 1000$ TeV for stability all the way to M_{Pl}, and one order of magnitude stronger than the quark ones if one requires only $\alpha_\lambda \geq 0$ at M_{Pl}. However, these constraints can be evaded by only one sizable Yukawa to one SM species, while assuming feeble ones for the other two SM generations. In this case, the models essentially resemble the ones in Sec. IV B.

V. CONCLUSIONS

For a decade, the Higgs has been fact and with it came the possibility of an unstable great desert (Fig. 1). We have considered avoiding the SM metastability as a primary model building task and put forward mechanisms for stability at the Planck scale. If a mechanism offers too little too late it will not lift the instability, while too much too soon can lead to unwanted singularities. In between, these constraints lead to stable, predictive, and testable BSM models including bounds for masses, couplings, and flavors.

A minimally invasive path to vacuum stability is given by the gauge portal mechanism, solely requiring SM-charged BSM fermions. The underlying interplay of couplings leads to a squeeze (Fig. 7) and an uplift (21) of the BSM Higgs quartic over the SM one. We showed that this mechanism works for all SM gauge interactions, i.e., strong, weak, hypercharge, and combinations thereof, with the electroweak portals a new addition of this work. In consequence, stability requires more flavors for larger masses; hence the closer the BSM mass is to the TeV scale, the more perturbative the gauge portal remains. All gauge portals are most efficient for lighter (TeV-scale) BSM fermions, where this minimal fix implies a weakly coupled, yet stable great desert.

Depending on the VLF representation, vacuum stability can require a range of flavor multiplicities as shown in Figs. 2, 5, 6, and 10 for various incarnations of the gauge portal. If Yukawa portals are unavailable, or too feeble, BSM fermions lead to long-lived particle signatures, such as diboson resonances, R hadrons if colored, or long-lived charged particles otherwise [94]. However, with already superfeeble Yukawas present, $\alpha_\kappa M_F \gtrsim 10^{-14}$ TeV [74], the BSM fermions decay promptly to SM particles and can be searched for experimentally with these signatures.

We also find that all 13 models with gauge portals and renormalizable Yukawa interactions to SM fermions and the Higgs (Table I) can become stable at the Planck scale, without prior Landau poles. Further, and except for model E which only features singlet BSM fermions, all models can generically become safe through both a gauge or a Yukawa portal. Interestingly, most models (except E, I, J, and L) can even be stabilized with a TeV-scale gauge portal (Table II). "Minimal" low-scale gauge portals, with a single generation of VLFs, feature stability with VLLs (models B, D, F) and VLQs (models K, M), as demonstrated in the upper plot of Fig. 14. The Yukawa portal stabilizes in a walking regime and allows all models to achieve stability minimally and with TeV-ish BSM masses (conditions compiled in Table III), as demonstrated in the lower plot of Fig. 14.

We find that models without a TeV-ish gauge portal (models E, I, J, and L) are subject to novel mass constraints, obtained from combining conditions for stability at the Planck scale with experimental search limits. The interplay of constraints is illustrated for models M and L in Figs. 14–16. Lower mass limits can improve search limits, see (29) (model L). If couplings to more than one SM generation are switched on, FCNC bounds can induce lower limits on M_F as strong as a few hundred TeV, see (30).

We also observe upper limits on fermion masses from stability, which are outside the reach of colliders.

We close with two remarks on how the gauge or Yukawa portal mechanism can be exploited for other purposes. The gauge portal lends itself naturally for the search of new GUTs or SM extensions with Higgs criticality. In fact, the mild modifications of the RG running of couplings can be used to search systematically for vacuum stability in combination with gauge coupling unification at or below the Planck scale. Also, having model building control over the gauge, Yukawa and Higgs couplings and their beta

functions at the Planck scale may prove useful to find extensions of the SM that connect successfully with quantized gravity [102]. Further directions include the exploration of cosmological consequences of our models. We hope to return to some of this in the future.

ACKNOWLDEGMENTS

This work is supported by the Studienstiftung des Deutschen Volkes (T. H.) and by the Science Technology and Facilities Council (STFC) Consolidated Grant No. ST/T00102X/1 (D. F. L.).

[1] CMS Collaboration, Observation of a new boson at a mass of 125 GeV with the CMS experiment at the LHC, Phys. Lett. B **716**, 30 (2012).
[2] ATLAS Collaboration, Observation of a new particle in the search for the Standard Model Higgs boson with the ATLAS detector at the LHC, Phys. Lett. B **716**, 1 (2012).
[3] G. Degrassi, S. Di Vita, J. Elias-Miro, J. R. Espinosa, G. F. Giudice, G. Isidori, and A. Strumia, Higgs mass and vacuum stability in the standard model at NNLO, J. High Energy Phys. 08 (2012) 098.
[4] D. Buttazzo, G. Degrassi, P. P. Giardino, G. F. Giudice, F. Sala, A. Salvio, and A. Strumia, Investigating the near-criticality of the Higgs boson, J. High Energy Phys. 12 (2013) 089.
[5] J. Elias-Miro, J. R. Espinosa, G. F. Giudice, H. M. Lee, and A. Strumia, Stabilization of the electroweak vacuum by a scalar threshold effect, J. High Energy Phys. 06 (2012) 031.
[6] M. Gonderinger, H. Lim, and M. J. Ramsey-Musolf, Complex scalar singlet dark matter: Vacuum stability and phenomenology, Phys. Rev. D **86**, 043511 (2012).
[7] L. A. Anchordoqui, I. Antoniadis, H. Goldberg, X. Huang, D. Lust, T. R. Taylor, and B. Vlcek, Vacuum stability of standard model^{++}, J. High Energy Phys. 02 (2013) 074.
[8] N. Arkani-Hamed, K. Blum, R. T. D'Agnolo, and J. Fan, 2:1 for naturalness at the LHC?, J. High Energy Phys. 01 (2013) 149.
[9] A. Joglekar, P. Schwaller, and C. E. M. Wagner, Dark matter and enhanced Higgs to di-photon rate from vector-like leptons, J. High Energy Phys. 12 (2012) 064.
[10] M. Fairbairn and P. Grothaus, Baryogenesis and dark matter with vector-like fermions, J. High Energy Phys. 10 (2013) 176.
[11] W. Altmannshofer, M. Bauer, and M. Carena, Exotic leptons: Higgs, flavor and collider phenomenology, J. High Energy Phys. 01 (2014) 060.
[12] E. Gabrielli, M. Heikinheimo, K. Kannike, A. Racioppi, M. Raidal, and C. Spethmann, Towards completing the Standard Model: Vacuum stability, EWSB and dark matter, Phys. Rev. D **89**, 015017 (2014).
[13] P. S. Bhupal Dev, D. K. Ghosh, N. Okada, and I. Saha, 125 GeV Higgs boson and the type-II seesaw model, J. High Energy Phys. 03 (2013) 150.
[14] A. Datta, A. Elsayed, S. Khalil, and A. Moursy, Higgs vacuum stability in the $B-L$ extended Standard Model, Phys. Rev. D **88**, 053011 (2013).
[15] N. Khan and S. Rakshit, Study of electroweak vacuum metastability with a singlet scalar dark matter, Phys. Rev. D **90**, 113008 (2014).
[16] R. Costa, A. P. Morais, M. O. P. Sampaio, and R. Santos, Two-loop stability of a complex singlet extended Standard Model, Phys. Rev. D **92**, 025024 (2015).
[17] V. V. Khoze, C. McCabe, and G. Ro, Higgs vacuum stability from the dark matter portal, J. High Energy Phys. 08 (2014) 026.
[18] M.-L. Xiao and J.-H. Yu, Stabilizing electroweak vacuum in a vectorlike fermion model, Phys. Rev. D **90**, 014007 (2014).
[19] C. Coriano, L. Delle Rose, and C. Marzo, Vacuum stability in U(1)-prime extensions of the standard model with TeV scale right handed neutrinos, Phys. Lett. B **738**, 13 (2014).
[20] S. Di Chiara, V. Keus, and O. Lebedev, Stabilizing the Higgs potential with a Z', Phys. Lett. B **744**, 59 (2015).
[21] N. Haba, H. Ishida, R. Takahashi, and Y. Yamaguchi, Hierarchy problem, gauge coupling unification at the Planck scale, and vacuum stability, Nucl. Phys. **B900**, 244 (2015).
[22] Z. Lalak, M. Lewicki, and P. Olszewski, Higher-order scalar interactions and SM vacuum stability, J. High Energy Phys. 05 (2014) 119.
[23] W. Altmannshofer, W. A. Bardeen, M. Bauer, M. Carena, and J. D. Lykken, Light dark matter, naturalness, and the radiative origin of the electroweak scale, J. High Energy Phys. 01 (2015) 032.
[24] G. Bélanger, K. Kannike, A. Pukhov, and M. Raidal, Minimal semi-annihilating $\mathbb{Z}_N$ scalar dark matter, J. Cosmol. Astropart. Phys. 06 (2014) 021.
[25] A. Salvio, A simple motivated completion of the standard model below the Planck scale: Axions and right-handed neutrinos, Phys. Lett. B **743**, 428 (2015).
[26] N. Chakrabarty, High-scale validity of a model with three-Higgs-doublets, Phys. Rev. D **93**, 075025 (2016).
[27] K. Blum, R. T. D'Agnolo, and J. Fan, Vacuum stability bounds on Higgs coupling deviations in the absence of new bosons, J. High Energy Phys. 03 (2015) 166.
[28] E. Bagnaschi, F. Brümmer, W. Buchmüller, A. Voigt, and G. Weiglein, Vacuum stability and supersymmetry at high scales with two Higgs doublets, J. High Energy Phys. 03 (2016) 158.
[29] M. Duch, B. Grzadkowski, and M. McGarrie, A stable Higgs portal with vector dark matter, J. High Energy Phys. 09 (2015) 162.

[30] M. Dhuria and G. Goswami, Perturbativity, vacuum stability, and inflation in the light of 750 GeV diphoton excess, Phys. Rev. D **94**, 055009 (2016).
[31] A. Salvio and A. Mazumdar, Higgs stability and the 750 GeV diphoton excess, Phys. Lett. B **755**, 469 (2016).
[32] M. Son and A. Urbano, A new scalar resonance at 750 GeV: Towards a proof of concept in favor of strongly interacting theories, J. High Energy Phys. 05 (2016) 181.
[33] Y. Hamada, K. Kawana, and K. Tsumura, Landau pole in the Standard Model with weakly interacting scalar fields, Phys. Lett. B **747**, 238 (2015).
[34] J. N. Ng and A. de la Puente, Electroweak vacuum stability and the seesaw mechanism revisited, Eur. Phys. J. C **76**, 122 (2016).
[35] A. Falkowski, C. Gross, and O. Lebedev, A second Higgs from the Higgs portal, J. High Energy Phys. 05 (2015) 057.
[36] H. Han and S. Zheng, New constraints on Higgs-portal scalar dark matter, J. High Energy Phys. 12 (2015) 044.
[37] M. Lindner, H. H. Patel, and B. Radovčić, Electroweak absolute, meta-, and thermal stability in neutrino mass models, Phys. Rev. D **93**, 073005 (2016).
[38] L. Delle Rose, C. Marzo, and A. Urbano, On the stability of the electroweak vacuum in the presence of low-scale seesaw models, J. High Energy Phys. 12 (2015) 050.
[39] A. Latosinski, A. Lewandowski, K. A. Meissner, and H. Nicolai, Conformal standard model with an extended scalar sector, J. High Energy Phys. 10 (2015) 170.
[40] D. Chowdhury and O. Eberhardt, Global fits of the two-loop renormalized two-Higgs-doublet model with soft Z_2 breaking, J. High Energy Phys. 11 (2015) 052.
[41] N. Khan and S. Rakshit, Constraints on inert dark matter from the metastability of the electroweak vacuum, Phys. Rev. D **92**, 055006 (2015).
[42] P. Ferreira, H. E. Haber, and E. Santos, Preserving the validity of the two-Higgs doublet model up to the Planck scale, Phys. Rev. D **92**, 033003 (2015).
[43] P. M. Ferreira and B. Swiezewska, One-loop contributions to neutral minima in the inert doublet model, J. High Energy Phys. 04 (2016) 099.
[44] B. Swiezewska, Inert scalars and vacuum metastability around the electroweak scale, J. High Energy Phys. 07 (2015) 118.
[45] C. Coriano, L. Delle Rose, and C. Marzo, Constraints on Abelian extensions of the standard model from two-loop vacuum stability and $U(1)_{B-L}$, J. High Energy Phys. 02 (2016) 135.
[46] S. Oda, N. Okada, and D.-s. Takahashi, Classically conformal U(1)' extended Standard Model and Higgs vacuum stability, Phys. Rev. D **92**, 015026 (2015).
[47] A. Das, N. Okada, and N. Papapietro, Electroweak vacuum stability in classically conformal B-L extension of the standard model, Eur. Phys. J. C **77**, 122 (2017).
[48] N. Haba and Y. Yamaguchi, Vacuum stability in the $U(1)_\chi$ extended model with vanishing scalar potential at the Planck scale, Prog. Theor. Exp. Phys. **2015**, 093B05 (2015).
[49] N. Haba, H. Ishida, R. Takahashi, and Y. Yamaguchi, Gauge coupling unification in a classically scale invariant model, J. High Energy Phys. 02 (2016) 058.
[50] A. Das, S. Oda, N. Okada, and D.-s. Takahashi, Classically conformal U(1)' extended standard model, electroweak vacuum stability, and LHC run-2 bounds, Phys. Rev. D **93**, 115038 (2016).
[51] N. Chakrabarty and B. Mukhopadhyaya, High-scale validity of a two Higgs doublet scenario: Metastability included, Eur. Phys. J. C **77**, 153 (2017).
[52] P. Bandyopadhyay and R. Mandal, Vacuum stability in an extended Standard Model with a leptoquark, Phys. Rev. D **95**, 035007 (2017).
[53] N. Khan, Exploring the hyperchargeless Higgs triplet model up to the Planck scale, Eur. Phys. J. C **78**, 341 (2018).
[54] N. Haba, H. Ishida, N. Okada, and Y. Yamaguchi, Vacuum stability and naturalness in type-II seesaw, Eur. Phys. J. C **76**, 333 (2016).
[55] Y. Mambrini, N. Nagata, K. A. Olive, and J. Zheng, Vacuum stability and radiative electroweak symmetry breaking in an SO(10) dark matter model, Phys. Rev. D **93**, 111703 (2016).
[56] W.-F. Chang and J. N. Ng, Renormalization group study of the minimal Majoronic dark radiation and dark matter model, J. Cosmol. Astropart. Phys. 07 (2016) 027.
[57] Y. Hamada, H. Kawai, K. Kawana, and K. Tsumura, Models of the LHC diphoton excesses valid up to the Planck scale, Phys. Rev. D **94**, 014007 (2016).
[58] D. K. Ghosh, N. Ghosh, I. Saha, and A. Shaw, Revisiting the high-scale validity of the type II seesaw model with novel LHC signature, Phys. Rev. D **97**, 115022 (2018).
[59] S. Oda, N. Okada, and D.-s. Takahashi, Right-handed neutrino dark matter in the classically conformal U(1)' extended Standard Model, Phys. Rev. D **96**, 095032 (2017).
[60] I. Garg, S. Goswami, K. N. Vishnudath, and N. Khan, Electroweak vacuum stability in presence of singlet scalar dark matter in TeV scale seesaw models, Phys. Rev. D **96**, 055020 (2017).
[61] P. Ghosh, A. K. Saha, and A. Sil, Study of electroweak vacuum stability from extended Higgs portal of dark matter and neutrinos, Phys. Rev. D **97**, 075034 (2018).
[62] S. Goswami, K. N. Vishnudath, and N. Khan, Constraining the minimal type-III seesaw model with naturalness, lepton flavor violation, and electroweak vacuum stability, Phys. Rev. D **99**, 075012 (2019).
[63] A. Dutta Banik, A. K. Saha, and A. Sil, Scalar assisted singlet doublet fermion dark matter model and electroweak vacuum stability, Phys. Rev. D **98**, 075013 (2018).
[64] P. Schuh, Vacuum stability of asymptotically safe two Higgs doublet models, Eur. Phys. J. C **79**, 909 (2019).
[65] C. Marzo, L. Marzola, and V. Vaskonen, Phase transition and vacuum stability in the classically conformal B–L model, Eur. Phys. J. C **79**, 601 (2019).
[66] S. A. R. Ellis, T. Gherghetta, K. Kaneta, and K. A. Olive, New weak-scale physics from SO(10) with high-scale supersymmetry, Phys. Rev. D **98**, 055009 (2018).
[67] S. M. Boucenna, T. Ohlsson, and M. Pernow, A minimal non-supersymmetric SO(10) model with Peccei–Quinn symmetry, Phys. Lett. B **792**, 251 (2019).
[68] S. Gopalakrishna and A. Velusamy, Higgs vacuum stability with vectorlike fermions, Phys. Rev. D **99**, 115020 (2019).

[69] J.-W. Wang, X.-J. Bi, P.-F. Yin, and Z.-H. Yu, Impact of fermionic electroweak multiplet dark matter on vacuum stability with one-loop matching, Phys. Rev. D **99**, 055009 (2019).
[70] N. Okada, D. Raut, and Q. Shafi, Inflation, proton decay, and Higgs-portal dark matter in $SO(10) \times U(1)_{\psi}$, Eur. Phys. J. C **79**, 1036 (2019).
[71] G. Hiller, C. Hormigos-Feliu, D. F. Litim, and T. Steudtner, Anomalous magnetic moments from asymptotic safety, Phys. Rev. D **102**, 071901 (2020).
[72] S. Bhattacharya, P. Ghosh, A. K. Saha, and A. Sil, Two component dark matter with inert Higgs doublet: Neutrino mass, high scale validity and collider searches, J. High Energy Phys. 03 (2020) 090.
[73] S. Mandal, R. Srivastava, and J. W. F. Valle, Consistency of the dynamical high-scale type-I seesaw mechanism, Phys. Rev. D **101**, 115030 (2020).
[74] G. Hiller, C. Hormigos-Feliu, D. F. Litim, and T. Steudtner, Model building from asymptotic safety with Higgs and flavor portals, Phys. Rev. D **102**, 095023 (2020).
[75] D. Borah, R. Roshan, and A. Sil, Sub-TeV singlet scalar dark matter and electroweak vacuum stability with vector-like fermions, Phys. Rev. D **102**, 075034 (2020).
[76] N. Chakrabarty, Doubly charged scalars and vector-like leptons confronting the muon $g-2$ anomaly and Higgs vacuum stability, Eur. Phys. J. Plus **136**, 1183 (2021).
[77] S. Mandal, R. Srivastava, and J. W. F. Valle, Electroweak symmetry breaking in the inverse seesaw mechanism, J. High Energy Phys. 03 (2021) 212.
[78] M. Fabbrichesi, C. M. Nieto, A. Tonero, and A. Ugolotti, Asymptotically safe SU(5) GUT, Phys. Rev. D **103**, 095026 (2021).
[79] A. Dutta Banik, R. Roshan, and A. Sil, Two component singlet-triplet scalar dark matter and electroweak vacuum stability, Phys. Rev. D **103**, 075001 (2021).
[80] P. Bandyopadhyay, S. Jangid, and A. Karan, Constraining scalar doublet and triplet leptoquarks with vacuum stability and perturbativity, Eur. Phys. J. C **82**, 516 (2022).
[81] R. Bause, G. Hiller, T. Höhne, D. F. Litim, and T. Steudtner, B-anomalies from flavorful U(1)′ extensions, safely, Eur. Phys. J. C **82**, 42 (2022).
[82] D. F. Litim and T. Steudtner, ARGES—advanced renormalisation group equation simplifier, Comput. Phys. Commun. **265**, 108021 (2021).
[83] Particle Data Group, Review of particle physics, Prog. Theor. Exp. Phys. **2020**, 083C01 (2020).
[84] V. Branchina, E. Messina, and M. Sher, Lifetime of the electroweak vacuum and sensitivity to Planck scale physics, Phys. Rev. D **91**, 013003 (2015).
[85] M. E. Machacek and M. T. Vaughn, Two loop renormalization group equations in a general quantum field theory. 3. Scalar quartic couplings, Nucl. Phys. **B249**, 70 (1985).
[86] A. G. Cohen and H. Georgi, Walking beyond the rainbow, Nucl. Phys. **B314**, 7 (1989).
[87] G. Cacciapaglia, C. Pica, and F. Sannino, Fundamental composite dynamics: A review, Phys. Rep. **877**, 1 (2020).
[88] A. V. Manohar, Introduction to effective field theories, arXiv:1804.05863.
[89] S. Weinberg, Effective gauge theories, Phys. Lett. B **91**, 51 (1980).
[90] ATLAS Collaboration, Determination of the strong coupling constant and test of asymptotic freedom from transverse energy-energy correlations in multijet events at $\sqrt{s} = 13$ TeV with the ATLAS detector, Report No. ATLAS-CONF-2020-025, 2020.
[91] A. D. Bond, G. Hiller, K. Kowalska, and D. F. Litim, Directions for model building from asymptotic safety, J. High Energy Phys. 08 (2017) 004.
[92] M. Farina, G. Panico, D. Pappadopulo, J. T. Ruderman, R. Torre, and A. Wulzer, Energy helps accuracy: Electroweak precision tests at hadron colliders, Phys. Lett. B **772**, 210 (2017).
[93] D. S. M. Alves, J. Galloway, J. T. Ruderman, and J. R. Walsh, Running electroweak couplings as a probe of new physics, J. High Energy Phys. 02 (2015) 007.
[94] M. M. Altakach, P. Lamba, R. Masełek, V. A. Mitsou, and K. Sakurai, Discovery prospects for long-lived multiply charged particles at the LHC, Eur. Phys. J. C **82**, 848 (2022).
[95] A. Falkowski and D. Straub, Flavourful SMEFT likelihood for Higgs and electroweak data, J. High Energy Phys. 04 (2020) 066.
[96] J. Ellis, M. Madigan, K. Mimasu, V. Sanz, and T. You, Top, Higgs, diboson and electroweak fit to the standard model effective field theory, J. High Energy Phys. 04 (2021) 279.
[97] K. Ishiwata, Z. Ligeti, and M. B. Wise, New vector-like fermions and flavor physics, J. High Energy Phys. 10 (2015) 027.
[98] ATLAS Collaboration, Combination of the Searches for Pair-Produced Vector-like Partners of the Third-Generation Quarks at $\sqrt{s} = 13$ TeV with the ATLAS Detector, Phys. Rev. Lett. **121**, 211801 (2018).
[99] ATLAS Collaboration, Overview of searches for single production of vector-like top and bottom quarks with the ATLAS experiment at 13 TeV, in *Proceedings of the 11th International Workshop on Top Quark Physics* (2018), arXiv:1811.11496.
[100] G. Hiller, T. Höhne, D. F. Litim, and T. Steudtner, Report No. DO-TH 22/17, 2022.
[101] J. A. Aguilar-Saavedra, R. Benbrik, S. Heinemeyer, and M. Pérez-Victoria, Handbook of vectorlike quarks: Mixing and single production, Phys. Rev. D **88**, 094010 (2013).
[102] M. Shaposhnikov and C. Wetterich, Asymptotic safety of gravity and the Higgs boson mass, Phys. Lett. B **683**, 196 (2010).